JCI The Journal of Clinical Investigation

Pathogenic variants in *TNNC2* cause congenital myopathy due to an impaired force response to calcium

Martijn van de Locht, … , Carsten G. Bönnemann, Coen A.C. Ottenheijm

J Clin Invest. 2021. https://doi.org/10.1172/JCI145700.

Research In-Press Preview **Genetics** **Muscle biology**

Graphical abstract

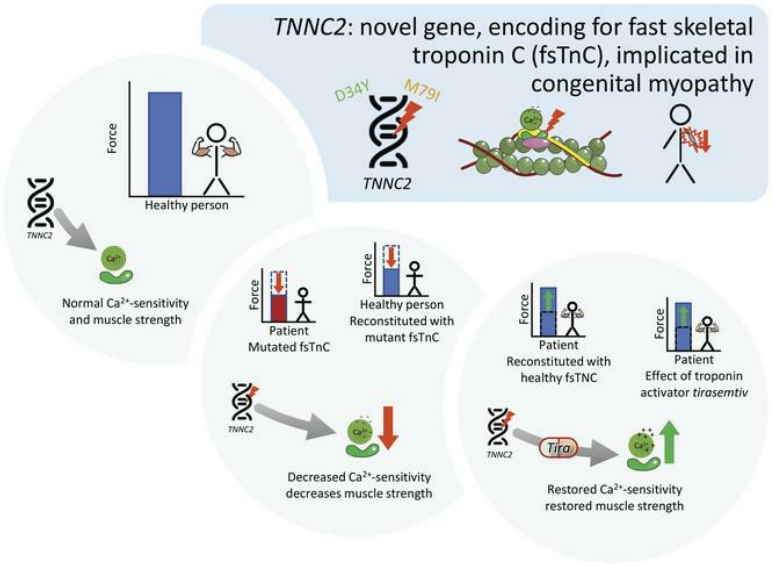

Find the latest version:

https://jci.me/145700/pdf

Pathogenic variants in *TNNC2* cause congenital myopathy due to an impaired force response to calcium

Martijn van de Locht[1], Sandra Donkervoort[2], Josine M. de Winter[1], Stefan Conijn[1], Leon Begthel[1], Benno Kusters[3], Payam Mohassel[2], Ying Hu[2], Livija Medne[4], Colin Quinn[5], Steven A. Moore[6], A. Reghan Foley[2], Gwimoon Seo[7], Darren T. Hwee[8], Fady I. Malik[8], Thomas Irving[9], Weikang Ma[9], Henk Granzier[10], Erik-Jan Kamsteeg[3], Kalyan Immadisetty[11], Peter Kekenes-Huskey[11], José R. Pinto[12], Nicol Voermans[3], Carsten G. Bönnemann[2 #], Coen A.C. Ottenheijm[1,10 #]

[1]Dept of Physiology, Amsterdam UMC, Amsterdam, The Netherlands; [2]Neuromuscular and Neurogenetic Disorders of Childhood Section, National Institute of Neurological Disorders and Stroke, National Institutes of Health, Bethesda, MD, USA; [3]Dept. of Neurology and Human Genetics, Radboud University Medical Center, Nijmegen, Netherlands; [4]Division of Human Genetics, Dept of Pediatrics, Individualized Medical Genetics Center, Children's Hospital of Philadelphia, Philadelphia, PA, USA; [5]Dept of Neurology, University of Pennsylvania, Philadelphia, PA, USA; [6]Dept of Pathology, University of Iowa Carver College of Medicine, Iowa City, IA, USA; [7]Protein Expression Facility, Institute of Molecular Biophysics, Florida State University, Tallahassee, FL, USA; [8]Research and Early Development, Cytokinetics Inc., South San Francisco, CA, USA; [9]BioCAT, Illinois Institute of Technology, Chicago, IL, USA; [10]Dept of Cellular and Molecular Medicine, University of Arizona, Tucson, AZ, USA; [11]Dept of Cell and Molecular Physiology, Loyola University, Chicago, IL, USA; [12]Dept of Biomedical Sciences, The Florida State University College of Medicine, Tallahassee, FL, USA

[#] Both authors contributed equally.

CORRESPONDING AUTHOR: Coen A.C. Ottenheijm, O|2 Labgebouw, De Boelelaan 1108, 1081 HZ, Amsterdam, (+31) (0)20 4448123, c.ottenheijm@amsterdamumc.nl

DISCLOSURE. We have no competing interest to disclose.

KEYWORDS. Troponin C, Sarcomere, Troponin activator, Congenital myopathy.

ABSTRACT

Troponin C (TnC) is a critical regulator of skeletal muscle contraction: it binds Ca^{2+} to activate muscle contraction. Surprisingly, the gene encoding fast skeletal TnC (*TNNC2*) has not yet been implicated in muscle disease. Here, we report two families with pathogenic variants in *TNNC2.* Patients present with a distinct, dominantly inherited congenital muscle disease. Molecular dynamics simulations suggest that the pathomechanisms by which the variants cause muscle disease include disruption of the binding sites for Ca^{2+} and for troponin I. In line with these findings, physiological studies in myofibers isolated from patients' biopsies revealed a markedly reduced force response of the sarcomeres to [Ca^{2+}]. This pathomechanism was further confirmed in experiments in which contractile dysfunction was evoked by replacing TnC in myofibers from healthy control subjects with recombinant, mutant TnC. Conversely, the contractile dysfunction of myofibers from patients was repaired by replacing endogenous, mutant TnC with recombinant, healthy TnC. Finally, we tested the therapeutic potential of the fast skeletal muscle troponin activator *tirasemtiv* in patients' myofibers and showed that the contractile dysfunction was repaired. Thus, our data reveal that pathogenic variants in *TNNC2* cause congenital muscle disease, and they provide therapeutic angles to repair muscle contractility.

INTRODUCTION

Skeletal muscle cells (myofibers) are densely packed with myofibrils, which consist of repeating structural units named sarcomeres (Fig.1A). Sarcomeres, the contractile units of muscle, are composed of thick filaments that contain the motor protein myosin and thin filaments composed of double helical strands of actin monomers, a coiled-coil dimer strand of tropomyosin and the troponin (Tn) complex (Fig.1B).

The Tn complex is a critical regulator of contraction. It is composed of three distinct subunits named according to their functions: a highly conserved Ca^{2+} binding subunit (TnC); an actomyosin ATPase inhibitory subunit (TnI) and a tropomyosin binding subunit (TnT). When muscle is activated, Ca^{2+} enters the cytosol, starting a molecular dance between the thick and thin filaments (1). First, Ca^{2+} binds to TnC, which initiates a chain of events in the other Tn subunits and leads to movement of the tropomyosin molecule, a process also modulated by myosin binding protein C (2). This movement exposes myosin binding sites on actin and allows the myosin heads on the thick filament to grab and pull on the actin molecules, thereby generating force. This ceaseless cycle is the mechanical basis for muscle contraction. Thus, TnC plays a 'gatekeeper' role in transmitting the Ca^{2+} signal to other sarcomere proteins to activate muscle contraction.

To date, the gene encoding fast skeletal troponin C (*TNNC2*; the skeletal muscle specific TnC isoform) has not been implicated in any muscle disease (myopathy). This is surprising, considering that TnC plays a key role in muscle contraction, and that nearly all other genes encoding key proteins in the sarcomere have been linked to disease, some already decades ago (3). Here, we resolve this enigma and report two unrelated families with pathogenic variants in *TNNC2.* Patients present with a distinct, dominantly inherited congenital myopathy, notable for polyhydramnios during gestational development, congenital weakness and severe respiratory muscle involvement with clinical improvement over time. The latter is atypical for congenital myopathy, which often has a static or progressive nature. Molecular dynamics (MD) simulations indicate that the *TNNC2* variants perturb the dynamics of the TnC regions

responsible for Ca^{2+} binding and for binding of the TnI switch peptide. In line with the findings from the MD simulations, studies in myofibers isolated from patients' biopsies revealed that the muscle weakness is caused by a reduced force response of the sarcomeres to submaximal $[Ca^{2+}]$. The pathogenicity of the variants was established in experiments, in which this contractile dysfunction was evoked by replacing endogenous TnC in myofibers from healthy control subjects with recombinant, mutant TnC. Conversely, we could repair the contractile dysfunction of myofibers from patients by replacing endogenous, mutant TnC with recombinant, healthy TnC. Finally, we tested the therapeutic potential of the fast skeletal muscle troponin activator *tirasemtiv* in patients' myofibers and showed that the contractile dysfunction was repaired.

RESULTS

Clinical presentation

Detailed clinical information for all patients is described in Table 1 and a full description of the patients is provided in the Supplemental Results section. Figure 2 shows family pedigrees, clinical and MRI images, and the visualization of muscle weakness (MuscleViz; based on the Medical Research Council grading). In brief, this disorder presents as a dominantly inherited myopathy with a characteristic clinical phenotype defining it as congenital in presentation. Distinct phenotypic characteristics include polyhydramnios during gestation, weakness and severe respiratory muscle involvement in the immediate postnatal period followed by clinical improvement over time with nonobligatory external ophthalmoparesis.

Identification of *TNNC2* variants

In both families, whole exome sequencing did not identify pathogenic variants in any of the known neuromuscular disease genes (details in Methods section). Subsequent analysis identified in Family 1 (P1, P2, P3) a heterozygous variant in *TNNC2*, encoding fast skeletal troponin C (fsTnC): c.100G>T; p.(Asp34Tyr); from here on referred to as D34Y. The variant was predicted to be damaging and was not present in dbSNP, NHLBI EVS or gnomAD (covering >125,000 individuals). The variant was confirmed through Sanger sequencing in P1, P2, and P3, and was absent in the unaffected family member. Thus, in Family 1 the *TNNC2* variant perfectly segregated with disease. Whole exome sequencing in Family 2 (P1) identified a heterozygous *de novo* variant in *TNNC2*: c.237G>C; p.(Met79Ile); from here on referred to as M79I. The variant was absent in both parents.

Conservation and location of the mutated TnC residues

GnomAD lists 71 rare missense variants in *TNNC2*, compared to the expected occurrence of 106, corresponding to a Z-score of 1.2. This lower than expected frequency of missense variants, with a positive Z-score, indicates increased intolerance of *TNNC2* to heterozygous

variation. In general, the amino acid sequence of fast skeletal troponin C (fsTnC) is highly conserved across species (for example, 99% conservation between humans and mice). The mutated residues are conserved across all species queried (Fig.1D). The location of both variants is indicated in Fig.1C-D, and in the protein 3D-structure (see below) of human fsTnC. The missense variant in F1, D34Y, is located in calcium binding site I where aspartic acid is replaced by a tyrosine residue (Fig.1C-D). Aspartic acid caries a hydrophilic acidic group with a negative charge. The replacing amino acid, tyrosine, does not carry a charge. The missense variant in F2, M79I, is located in an α-helix next to calcium binding site II where methionine is replaced by isoleucine, both neutral (Fig.1C-D).

Muscle (ultra)structure

Structure. From patient 1 of family 1 (F1:P1) and patient 1 of family 2 (F2:P1), muscle biopsies were obtained and used for analyses of muscle (ultra)structure. Hemotoxylin and eosin (H&E) stained sections showed a slight variation in myofiber size in both patients (Fig.3A-B). There was no evidence of necrosis, degeneration, inflammation or fibrosis. Immunohistochemical staining for dystrophin-glycoprotein associated proteins was normal (images not shown). No nemaline rods or inclusions were observed in Gömöri trichrome stained sections of both patients (Fig.3C-D). NADH stained sections showed occasional, scattered atrophic fast twitch myofibers (Fig.3E-F). Analysis of myofiber size (minFeret) in both patients showed hypertrophy of slow twitch myofibers and normally sized fast twitch myofibers compared to control subjects (Fig.3G; Table 3; note that basic demographic information of the control subjects is shown in Table 2). The proportion of slow twitch fibers was slightly higher in F1:P1 compared to controls. Fiber type proportion in F2:P1 was comparable to controls (Fig.3H; Table 3).

***Ultrastructure*.** Electron microscopy showed preserved, intact myofibrillar ultrastructure in myofibers of both patients (Fig.3I-J). To study the structure of the thin filaments in the myofibrils, we performed experiments at the Advanced Photon Source (Argonne, IL, USA). Low-angle X-ray diffraction patterns were obtained from preparations in which 28 myofibers

were mounted and aligned in a single plane between 2 halves of EM grids (methods described in De Winter et al., 2020; schematic in Supplemental Fig.S1) (4). This approach allowed for high-quality meridional diffraction patterns in relaxed muscle fibers (for example, see Fig.3K). Because *TNNC2* is expressed in fast twitch myofibers only, we aimed at comparing fast twitch and slow twitch fibers within a muscle biopsy of a patient. This approach was only feasible in F1:P1, as in this biopsy we could segregate fiber types based on visual inspection and produce grids with only slow twitch myofibers and grids with only fast twitch myofibers (Fig.3K, bottom). The actin layer line 6 (ALL6), indicating the left-handed pitch of the thin filament helix, and the Tn3 reflection, representing the spacing of troponin complexes on the thin filament, were comparable between fast- and slow twitch fibers (Fig.3L&M). Thus, the low-angle X-ray diffraction studies suggest that the D34Y variant in *TNNC2* does not affect the structure of the thin filament in fast twitch myofibers.

Molecular dynamics simulations

To study the effects of the variants in *TNNC2* on the structure and dynamics of fsTnC proteins, we performed 18 μs molecular dynamics (MD) simulations. Simulations were performed for human fsTnC. In our analyses, we focused on the N-terminal domains of fsTnC, as these are critical for thin filament activation during excitation-contraction coupling in skeletal muscle. In short, TnC binds Ca^{2+} at sites I and II in its N-terminal domains (Fig.1C & 4B). Site I is a Ca^{2+}-binding loop (or EF-hand) formed by residues 27–37 and site II is a Ca^{2+}-binding loop formed by residues 64 to 74. During Ca^{2+} binding, the loops undergo a conformational change to coordinate Ca^{2+}, which then promotes the opening of a hydrophobic pocket on the TnC solvent-exposed surface. This ‘open’ structure is accompanied by higher mobility in residues 45-55, which correspond to regions in helices B and C that accommodate binding of the TnI switch peptide. Binding of the TnI switch peptide results in downstream conformational changes in the thin filament that ultimately facilitate the binding of myosin to actin (5–7). Figure 4A&B show

the MD-predicted structure of the N-domains of wild-type and mutated fsTnC, in both the apo (no Ca^{2+} bound) and holo state (Ca^{2+} bound).

Root mean squared fluctuations. First, we assessed the structural dynamics for each amino acid of WT-, D34Y-, and M79I-fsTnC via root mean squared fluctuations (RMSF). In Fig.4C&D, the RMSF are restricted to the N-terminal domain, which isolates the effects of Ca^{2+} binding on the mobility of the domain's helices. In the apo state, WT-fsTnC had high RMSF in the Ca^{2+} binding loops, which were significantly reduced upon Ca^{2+} binding (holo state). Thus, Ca^{2+} binding stabilized the loops. While a similar reduction in RMSF upon Ca^{2+} binding was observed in the CD loops of D34Y-fsTnC, the D34Y variant rendered the AB loops more mobile in the holo state relative to the apo state (Fig.4C). The presence of the M79I variant promoted greater mobility of the AB loops in the holo state relative to the apo state (Fig.4D), albeit to a lesser extent than the D34Y variant. The M79I variant greatly increased the mobility of residues 45-55, the region that binds TnI switch peptide. Thus, these MD simulations predict that the D34Y and M79I variants in fsTnC perturb the dynamics of regions important for Ca^{2+} binding, while the M79I variant affects the binding of the TnI switch peptide in addition.

Ca^{2+} coordination in holo structures. The binding of Ca^{2+} to EF hands is determined to a large extent by the number and position of oxygen residues in the Ca^{2+} binding loop (8, 9). We therefore examined the spatial arrangement of the oxygens that bind Ca^{2+} in the AB and CD loops. Both loops exhibit maxima in the radial distribution functions (RDFs) at ~2.3Å (Fig.4E&G). In the AB loop, the D34Y variant reduces the number of coordinating oxygens (2.5 vs. 6, respectively; Fig.4E), which likely causes the greater mobility in this region, as measured by RMSF. The M79I variant caused a negligible reduction in coordinating oxygens (Fig.4E). Both variants resulted in fewer water molecules leaving the Ca^{2+} coordination shells relative to WT (Fig.4F), which is indicative of a decreased ability of the protein to desolvate the ion. The changes in coordination structure, in particular those caused by the D34Y variant, are likely to impact the binding thermodynamics of Ca^{2+} to the first EF hand.

Structure and dynamics of the fsTnC hydrophobic pocket. The simulation data suggest

194 that the variants affect the region spanning residues 45-55 (B/C helices). This region is
195 displaced during Ca^{2+} binding to open a hydrophobic pocket that can subsequently bind the
196 TnI switch peptide (10). To quantify these effects, we used principal component analysis
197 (PCA). Two principal components (PC)s account for >60% of the variance, or conformation
198 changes, in our simulated structures (Fig.4I). PC1 captures the displacement of helices B and
199 C (see per-residue contribution to PC1 in Fig.4J), which drives the opening of the hydrophobic
200 pocket following binding of Ca^{2+} to the EF hands. To a lesser extent, PC1 captures the
201 rearrangement of the Ca^{2+} binding loops in the holo state. Upon projection of the simulation
202 data into the PC1 basis, the WT apo state assumes more negative values, while its holo state
203 yields more positive values (Fig.4I). In other words, the WT holo state generally features a
204 more open hydrophobic pocket than the apo state. The PC1 projections for both apo and holo
205 states of D34Y-fsTnC are markedly different from those for WT-fsTnC (Fig.4I). This is likely a
206 consequence of both the AB loop and the helices B/C being perturbed relative to the WT. We
207 speculate that these effects of D34Y impede the exposure of the hydrophobic pocket,
208 necessary for binding the TnI switch peptide.
209 The projections for the M79I-fsTnC apo and holo states are comparable to that of WT-fsTnC.
210 PC2, which describes the contraction of the AB and CD loops upon Ca^{2+} binding (Fig.4J), show
211 no major effect of the variants (Fig.4I).
212 ***Effects beyond the coordination regions and the hydrophobic pocket.*** Fig.4D showed
213 that the M79I variant enhanced the mobility of the B/C helices, but this did not manifest in
214 significant structural changes relative to WT based on our PC analysis. We therefore examined
215 whether the substitution of the isoleucine at position 79 induces subtle changes in the
216 hydrophobic patch that could impinge on the binding of the TnI switch peptide. We used the
217 cardiac TnC/TnI complex (PDB 1MXL) to approximate the binding pose of the TnI switch
218 peptide in fsTnC. Fig.4K shows the cTnC/TnI complex superimposed onto fsTnC. The cardiac
219 TnI position is accommodated into the fsTnC hydrophobic pocket without introducing
220 unfavorable steric overlap between the proteins. The isoleucine side chain does not present

any steric overlaps with the cTnI peptide. However, among the amino acids that are directly adjacent to both TnI and the M79 position, I59, F76, M80, R82, and Q83 are displaced by roughly 2Å. Thus, the M79I variant appears to reorganize the hydrophobic patch configuration. In an effort to test the hypothesis that the M79I variant perturbs the TnC and TnI interaction, we simulated an intact troponin complex comprising TnC, TnI and TnT. For this purpose we simulated via all atom MD (Supplemental Fig.S2, panel A) the holo forms of the WT and M79I variants, based on structural data for the human cardiac Tn complex (PDB 1J1E), as analogous structural data for the skeletal muscle isoforms have not been reported (11). The MD data suggest that the M79I variant perturbs the TnI interaction with the N-domain of TnC. This is evident as a displacement of the interacting TnI peptide in the presence of the M79I variant relative to its position in the presence of the WT (Supplemental Fig.S2, panel B). Our data indicate that this displacement may be due to the pathogenic variant forming a new contact between TnC-I79 and TnI-M155 that is not evident in WT TnC. This difference may arise of an alternate side chain placement of TnI-V148 (Supplemental Fig.S2, panel B). Although structural data are not available to validate this prediction, the finding of a displaced TnI inhibitory peptide for the M79I variant is consistent with our hypothesis that M79I alters TnI/TnC interactions.

Thus, altogether, the MD simulations suggest that the D34Y variant has the most significant impact on the fsTnC structure, by affecting the displacement of the first N-terminal EF hand following Ca^{2+} binding, the coordination of Ca^{2+} binding by oxygens, and impeding the exposure of the hydrophobic pocket, to which the TnI switch peptide binds. The M79I variant has more modest effects that manifest in greater mobility of the fsTnC B/C helices following Ca^{2+} binding and may interfere with the fsTnC/fsTnI switch peptide interface. These effects of the *TNNC2* variants on the structure and dynamics of fsTnC might impact the calcium sensitivity of force generation of sarcomeres.

Myofiber contractility

Force production and calcium sensitivity

To study whether the structural changes in mutated fsTnC impair the contractility of sarcomeres, we isolated myofibers from the patients' biopsies using microforceps. Myofibers were permeabilized, exposed to incremental [Ca^{2+}] solutions, and the force generated was recorded (Fig.5A-B). To account for differences in myofiber size, absolute maximal force was normalized to the CSA of the myofiber to obtain specific force. In both patients, the maximal specific force of slow twitch and fast twitch myofibers was comparable to that of myofibers from control subjects (Fig.5E). Thus, these findings indicate the *TNNC2* variants do not affect the maximal force generating capacity of the sarcomeres.

In Fig.5C, the force-[Ca^{2+}] relations are shown of slow twitch and fast twitch myofibers of control subjects, F1:P1, and F2:P1. Slow twitch myofibers show no differences in the force-[Ca^{2+}] relation between groups. However, in fast twitch myofibers of F1:P1 and F2:P1, the force-[Ca^{2+}] relation is markedly shifted rightwards, indicating a lower Ca^{2+} sensitivity of force. The rightward shift of the force-[Ca^{2+}] relation is illustrated by the higher $[Ca^{2+}]_{50}$, i.e. the [Ca^{2+}] at which 50% of maximal force is produced (F1:P1: Δ = +2.59 µM, $p < 0.001$; F2:P1: Δ = +1.35 µM, $p < 0.001$). This indicates that in patients' myofibers more Ca^{2+} is required to generate 50% of maximal force production (Fig.5D).

Thus, the major phenotype of the myofibers of the patients with *TNNC2* variants is a markedly reduced calcium sensitivity of force in fast twitch myofibers.

Reconstitution of myofibers with fast skeletal TnC

To study whether the reduced calcium sensitivity of force in patients' myofibers is a direct cause of the presence of mutant fsTnC in the sarcomeres, we studied whether replacing the endogenous, mutant fsTnC with recombinant, wild-type fsTnC would restore the contractile function of patients' myofibers. In brief, permeabilized fast twitch myofibers were exposed to an extraction solution, removing endogenous fsTnC. Hereafter, recombinant fsTnC was introduced into these myofibers (Fig.6A). We did not assess the level of incorporation of mutant

proteins, but we did measure the maximal force production of myofibers before extraction (baseline force), after extraction of endogenous fsTnC, and after reconstitution with exogenous fsTnC. Successful extraction of endogenous fsTnC from the myofibers of control subjects and patients was assumed based on the reduced maximal force generation of extracted myofibers (Table S1), and successful reconstitution with endogenous fsTnC was indicated by the restoration of maximal force (Table S1). Thus, the stage was set to test the effect of the *TNNC2* variants on the force-[Ca^{2+}] relation in myofibers.

Before extraction and after reconstitution of the myofibers with recombinant fsTnC, the force-[Ca^{2+}] relation was determined (Fig.6B-E) to assess the calcium sensitivity of force generation. Reconstitution of myofibers of controls with WT-fsTnC did not affect the calcium sensitivity of force (Fig.S3; Table S2). This indicates that the protocol used for the extraction and reconstitution had no adverse effects on the contractility of myofibers. Interestingly, reconstitution of myofibers of controls with D34Y-fsTnC or M79I-fsTnC decreased the calcium sensitivity of force (Fig.6B&C, respectively; Table S2): after reconstitution with D34Y-fsTnC, 80% more Ca^{2+} was required to generate 50% of maximal force; after reconstitution with M79I-fsTnC, 137% more Ca^{2+} was required (Fig.6B&C, insets; Table S2). Thus, we could successfully evoke the patients' phenotype in myofibers of healthy controls by replacing endogenous fsTnC with exogenous, mutated fsTnC.

Next, we performed the opposite experiment, i.e. replacing mutant fsTnC in the patients' myofibers with WT-fsTnC. After reconstituting the F1:P1 myofibers with WT-fsTnC, the calcium sensitivity of force was restored to control values (Fig.6D; Table S2). This was also observed after reconstituting F2:P1 myofibers with WT-fsTnC (Fig.6E; Table S2). We also reconstituted F1:P1 myofibers with a 50/50 mixture of WT- and D34Y-fsTnC and observed an increase of the calcium sensitivity of force (Tables S1&S2), with a $\Delta[Ca^{2+}]_{50}$ which was ~50% of the increase after reconstitution with 100% WT-fsTnC. Reconstitution of F2:P1 myofibers with a 50/50 mixture of WT- and M79I-fsTnC did not increase the calcium sensitivity of force (Tables

S1&S2). These findings support the dominant effect of the variants, with the most profound effect elicited by the M79I variant.

Thus, reconstituting healthy human myofibers with D34Y-fsTnC or M79I-fsTnC decreases the calcium sensitivity of force, while reconstituting patient myofibers with WT-fsTnC increases the calcium sensitivity of force back to normal values. These findings indicate that we can mimic the patients' phenotype in control myofibers by reconstitution with D34Y- and M79I-fsTnC, and repair the calcium sensitivity of force in patients' myofibers by reconstitution with WT-fsTnC. These experiments conclusively establish the pathogenicity of the variants in *TNNC2*.

Effect of tirasemtiv on myofiber contractility

Tirasemtiv was used to study the ability of a fast skeletal muscle troponin activator to repair the contractility of patients' fast twitch myofibers. In brief, permeabilized fast twitch myofibers isolated from patients' muscle biopsies were exposed to various Ca^{2+} solutions in the absence and presence of 10 µM *tirasemtiv* (Fig.7A). This concentration was selected based on previous work from our group (12). In fast twitch fibers of both F1:P1 and F2:P1, *tirasemtiv* restored the calcium sensitivity of force to control values (Fig.7B-C, respectively; Table S3). We also tested the effect of *tirasemtiv* on slow-twitch myofibers, data are in online methods. Note that, unexpectedly, *tirasemtiv* also increased the maximal force of F1:P1 fast twitch myofibers, and this was also observed in F2:P1, although to a lesser extent; the magnitude of maximal force increase induced by *tirasemtiv* correlated with the magnitude of the increase of the pCa_{50} of the patient fibers relative to control values (Supplemental Fig.S4). Fibers of control subjects showed no increase of maximal force in response to *tirasemtiv* (Supplemental Fig.S4C). Thus, *tirasemtiv* increased the force generated by patients' myofibers at physiological $[Ca^{2+}]$ to that generated by control myofibers.

DISCUSSION

This study reports variants in *TNNC2,* the gene encoding fast skeletal troponin C, as a cause of human disease. Two missense variants were identified in unrelated families (c.100G>T, D34Y; c.237G>C, M79I). Patients from both families presented with a distinct and recognizable phenotype of congenital weakness in combination with severe congenital respiratory insufficiency. This phenotype improved over time, allowing for ambulation and respiratory independence, which is atypical for congenital myopathies which often have a static or progressive nature. Other notable features include facial weakness, ptosis, decreased extraocular movements and jaw contractures.

We provide strong evidence for pathogenicity of the *TNNC2* variants. Because the calculation of a conclusive LOD (logarithm (base 10) of odds) score of > 3.0 was not possible due to the limited number of scorable meiosis in Family 1, we obtained several layers of additional evidence. As noted, the pedigree analysis in Family 1 showed perfect segregation of the variant with disease in three generations under dominant inheritance and full penetrance, while the patient in Family 2 has a *de novo* variant in *TNNC2* (paternity and maternity confirmed) with no family history of muscle disease, compatible with pathogenicity of the variants. Furthermore, during the past years, we have exome sequenced ~1400 patients with neuromuscular disease, and never identified patients with variants in *TNNC2*, except the patients presented here. These variants have also never been documented in the 125,000 person gnomAD cohort of normal individuals, consistent with their pathogenicity in the heterozygous state. Also, the clinical phenotype in both families is highly unusual and entirely consistent between the two families, who on our analysis only share the *TNNC2* variants and do not have variants in any of the other established myopathy genes. Finally, we provide experimental functional evidence supporting pathogenicity: MD simulations indicated that the location of the variants affects the structure of the protein product and might impair the force response of myofibers to submaximal Ca^{2+} concentrations, which was confirmed in functional

assays in patients' myofibers. Importantly, the contractile phenotype in patients' myofibers was repaired by replacing the mutant fsTnC with recombinant wild-type fsTnC (Fig.6D&E). Conversely, the contractile phenotype was evoked by replacing fsTnC in myofibers from healthy control subjects with recombinant, mutant fsTnC (Fig.6B&C). According to the variant classification criteria of the American College of Medical Genetics and Genomics (13) these multiple layers of evidence, including experimental functional evidence, classify the *TNNC2* variants as pathogenic (Family 1: PS3, PM2, PP3; Family 2: PS2, PS3, PM2, PP3).

Thin filament-associated protein disorders define a subgroup of congenital disorders of muscle, including those associated with variants in troponin T (*TNNT1* (14) and *TNNT3* (15)), alpha-actin 1 (*ACTA1*) (16), alpha- and beta-tropomyosin (*TPM3* and *TPM2*) (17, 18), nebulin (*NEB*) (19), leiomodin-3 (*LMOD3*) (20), cofilin 2 (*CFL2*) (21), unconventional myosin 18B *(MYO18B)* (22), myopalladin (*MYPN*) (23), kelch family members 40 (*KLHL40*) and -41 (*KLHL41*) (24, 25), and kelch repeat and BTB (POZ) Domain Containing 13 (*KBTBD13*) (26), but not yet in *TNNC2*. Many of these disorders histologically feature nemaline rods as the defining characteristic of nemaline myopathies, which were notably absent in myofibers of F1:P1 and F2:P1 (Fig.3). We acknowledge, however, that there are many other examples of mutations in 'nemaline myopathy' genes without nemaline rods, and it is entirely possible that there are nemaline rods somewhere in certain muscles/fibers that were however not sampled in the patients studied here. Another remarkable feature of the *TNNC2*-related myopathy described here is the subsequent clinical improvement in strength and respiratory function following the severe postnatal respiratory insufficiency and weakness in all four patients. While some degree of clinical improvement may occur in patients with congenital myopathy, the degree to which the patients with *TNNC2*-related myopathy improved is highly unusual. Thus, variants in *TNNC2* cause a distinct congenital phenotype. The basis of the clinical improvement might relate to the switch from predominantly fast twitch (*TNNC2*-expressing) myofibers in muscles after birth to a 50/50 distribution of slow- and fast twitch myofibers at

older age (27). Hence, with age-related muscle maturation, this switch towards more slow twitch myofibers might help compensate for the initially more pronounced pathogenic effect of the *TNNC2* variants. Human laryngeal myofibers rely on fast isometric contractions for proper respiration and airway protection so that the prominent stridor contributing to the early respiratory failure might be attributable to this (28). It is, however, unclear whether there are postnatal developmental changes in myofiber type composition that make laryngeal muscles less dependent on fsTnC, and thus account for the unusual clinical improvement in respiratory function. Of note, a fast-to-slow fiber type switch does not occur in the extraocular muscles, which continue to be affected in the patients. Slow twitch myofibers should be able to compensate effectively as they are spared functionally, generating normal force (Table 4), as well as histologically in that we observed a mild hypertrophy of slow twitch myofibers (Fig.3) and not the slow twitch myofiber atrophy and predominance that is a feature commonly seen in the nemaline myoapthies (3). Furthermore, during daily life activities, the affected fast twitch myofibers are recruited to a much lesser degree than the spared slow twitch myofibers (Henneman's size principle). Consequently, the relatively low activity level of fast twitch myofibers might facilitate timely turnover of mutant protein in the myofibers and prevent disease progression. These mechanisms might also underlie the reported improvement with age of the clinical phenotype of patients with mutations in other 'fast twitch muscle genes' such as *TNNT3* (29, 30).

TNNC2 is highly conserved across species, including the sequence close to the variants reported here (Fig.1D). Both variants found in the two families act in a heterozygous dominant manner, so that both wild-type and mutant protein are expected to be expressed in myofibers. Our studies indicate that mutant proteins were incorporated in the thin filaments, as replacing endogenous fsTnC in patients' myofibers with wild-type recombinant fsTnC completely restored the contractile phenotype (Fig.6). Furthermore, it is unlikely that haploinsufficiency

contributed to the contractile phenotype, as that should have compromised the maximal force generating capacity of the myofibers, which was not observed (Table 4).

In contrast to many other congenital myopathies genes (3), variants in *TNNC2* do not appear to cause muscle weakness by myofiber atrophy (Fig.3G) or by damaged myofibrillar ultrastructure (Fig.3I-M). Indeed, the maximal force generating capacity of fast twitch myofibers, isolated from patents' biopsies, was similar to those isolated from biopsies of control subjects (Table 4). The findings from the contractility assays in permeabilized myofibers, assays in which possible confounding effects of Ca^{2+} handling by the sarcoplasmatic reticulum are absent, revealed that the muscle weakness is primarily caused by a strong reduction in the Ca^{2+} sensitivity of force generation by the sarcomeres (Fig.5). The sarcomeres in fast twitch myofibers of F1:P1 required 3-fold more Ca^{2+} to generate fifty percent of maximum force, whereas myofibers of patient F2:P1 required 2-fold more Ca^{2+}. Note that this more pronounced phenotype in F1:P1 at the myofiber level at least partly explains the more severe clinical phenotype of patients with the D34Y variant compared to the patient with the M79I variant. The pathogenicity of the variants was established in experiments in which the contractile phenotype was evoked by replacing endogenous fsTnC in myofibers from control subjects with recombinant, mutant fsTnC (Fig.6). Conversely, we could repair the contractile phenotype of myofibers from patients by replacing endogenous, mutant fsTnC with recombinant, healthy fsTnC (Fig.6). The MD simulations suggested two different molecular mechanisms for the D34Y and M79I variants that underlie the reduced Ca^{2+} sensitivity of force. The D34Y variant had the most pronounced effect on fsTnC and might change the displacement of the first N-terminal EF hand following Ca^{2+} binding and impede the exposure of the hydrophobic pocket to which the TnI switch peptide binds. The MD simulations suggested a more subtle effect from the M79I variant, which might directly impinge on the binding of the TnI switch peptide by displacing residues I59, F76, M80, R82, and Q83 by 2Å. These residues constitute part of the solvent-exposed hydrophobic patch that interfaces with the TnI switch peptide. Indeed,

simulations of the intact troponin complex comprising TnC, TnI and TnT, suggested that the M79I variant perturbs the placement of the TnI inhibitory peptide (Supplemental Fig.S2). Since the binding of the TnI switch peptide is a requisite step in force generation that directly follows Ca^{2+} binding in the fsTnC N-terminal domain, it is plausible that the variants considered in this study may interfere with the TnC/TnI interaction. The more pronounced effects of the D34Y variant on fsTnC dynamics, relative to those of M79I, are in line with the larger reduction in the calcium sensitivity of force in patient F1:P1 relative to F2:P1 (Fig.5). Whether the *TNNC2* variants, and in particular the D34Y variant, impact the binding of Ca^{2+} to fsTnC, as the MD simulations suggest, should be addressed in future studies.

Therapeutic approaches to a *TNNC2*-related myopathy include the competitive introduction of wild-type fsTnC in patients' muscles by AAV gene therapy. Recent advances show the potential of AAV vectors in gene therapy for neuromuscular diseases, and AAV vector-mediated gene delivery was recently approved for spinal muscular atrophy (31–33). Our *in vitro* results suggest that competing off the mutant fsTnC with wild-type fsTnC results in correction of the contractile phenotype. However, targeting wild-type *TNNC2* to fast twitch muscle fibers only is one of the challenges that would need to be met. Using a small molecule strategy to target the physiological consequences of the variant rather than the variant itself, is another potentially valid approach to address this condition. In the present study we tested the ability of the small molecule fast skeletal muscle troponin activator *tirasemtiv*, to augment the force response to calcium in myofibers of patients. *Tirasemtiv* binds to fsTnC and amplifies the response of the thin filament to calcium in fast twitch myofibers, leading to increased muscle force at submaximal rates of nerve stimulation (34). Thus, fast skeletal muscle troponin activation might offer a feasible therapeutic approach in patients with *TNNC2* variants. In our studies we tested the effect of 10 µM *tirasemtiv*, a concentration we have used in previous work and which elicits a maximal force response without affecting the relaxation kinetics of myofibers (12). Although a relatively high concentration, it is considerably lower than the TnC

concentration in skeletal muscle, and, furthermore, *tirasemtiv* is specific for fsTnC and does not bind elsewhere in the sarcomere to activate muscle (34, 35). Importantly, at physiological calcium concentrations, the force generated by patients' myofibers increased by up to 600% in the presence of *tirasemtiv*, and reached values that were close to or even higher than those of healthy subjects (Fig.7). An interesting observation was that *tirasemtiv* not only increased the force response to submaximal calcium concentrations, but also to saturating calcium concentrations (~40%; Suppl. Fig.S3). This effect was not observed in previous studies with *tirasemtiv* (eg., Russell et al. (34) and Hwee et al. (2014) (36); although Lee et al. (37) showed a ~7% increase). We speculate that this effect relates to *tirasemtiv* binding to the interface of TnC/TnI (34). The *TNNC2* variants induce structural alterations in/near this interface (Fig.4), and might enhance the effect of *tirasemtiv* on the Ca^{2+} off rates, even at saturating calcium concentration. Although, *tirasemtiv* did not meet its primary endpoint in a recent phase 3 clinical trial in amyotrophic lateral sclerosis patients in part to tolerability (including dizziness, fatigue, nausea, weight loss and insomnia) (38), our findings illustrate the great therapeutic promise of fast skeletal muscle troponin activation. *Reldesemtiv*, a second generation fast skeletal muscle troponin activator that is structurally distinct from *tirasemtiv*, has a lower side effect profile and is currently under clinical trial investigation (39, 40).

In summary, we characterized two families with a distinct congenital myopathy caused by dominantly acting variants in *TNNC2.* Recognition of the *TNNC2*-related phenotype reported here may facilitate early diagnosis and management. Furthermore, by combining molecular dynamics simulations and myofiber contractility studies, we showed that the disease mechanism of *TNNC2*-related myopathy is driven by a reduction in the calcium sensitivity of force (graphic summary in Fig.8), thus providing a potential promising avenue for therapeutic intervention.

METHODS

A summary of the methods applied is described below. Additional details are in the online supplement.

Patient Recruitment and Sample Collection

Patients' and control subjects' general information are in Table 2. A detailed clinical description of both patients' families is in Table 1. Additional details of human study approval, informed consent, and image approval can be found below in the study approval section and further details of recruitment and sample details are in the online supplement.

Genetic testing

Whole exome sequencing (WES) was performed on genomic DNA extracted from blood. WES on patients F1:P1, F1:P2 and F1:P3 was performed through the NIH Intramural Sequencing Center (NISC) using the Nimblegen SeqCap EZ Exome +UTR Library and Illumina HiSeq 2500 sequencing instruments. WES data was analyzed using an exome-based targeted panel approach (exome slice) to identify variants in known neuromuscular disease genes, with subsequent reflex analysis of all WES generated data. Pathogenicity was assessed using the American College of Medical Genetics and Genomics (ACMG)/Association for Molecular Pathology (AMP) guidelines for interpretation of sequence variants, which includes population data, computational and predictive data using various lines of computational evidence (CADD, Polyphen, Sift) and segregation data (13). Variants were also analysed using Varsifter and searched for in dbSNP and NHLBI EVS (41, 42). The *TNNC2* variant was confirmed by Sanger sequencing in F1:P1, F1:P2 and F1:P3, and in unaffected relatives F1:U1 and F1:U2 using DNA extracted from saliva. DNA from P3's parents was not available for segregation testing. WES on F2:P1 and her parents (trio-based sequencing) was performed by the Beijing Genome Institute Europe (Copenhagen, Denmark) using an Illumina HiSeq 4000 after enrichment for exons using the Agilent SureSelectXT Human All Exon 50Mb Kit (version 5). Read alignment

(BWA), variant calling (GATK), variant annotation and interpretation of variants were done by the department of Genetics at the Radboudumc. Note that in F2:P1 a second variant was found in a non-coding region (intron) of HAP1 (this variant is often found in WES, suggesting that it is a sequencing artifact).

Immunohistochemistry

For F1:P1, NADH staining was used to quantify the cross-sectional area (CSA) of the slow twitch and fast twitch myofibers. For control subjects and F2:P1 a mATPase 4.2 staining was used to quantify the CSA. To analyze the cross-sections, open source Fiji software was used to manually trace the circumference of the myofibers and calculate the Feret diameter (43).

Low-angle X-ray diffraction

Low-angle X-ray diffraction experiments were performed on the Biophysics Collaborative Access Team beamline 18ID at the Advanced Photon Source, Argonne National Laboratory, Argonne, IL (44). From patient F1:P1, twenty-eight fibers were mounted and aligned in one plane between two-halves of an electron microscopy grid and X-ray diffraction patterns were collected at a sarcomere length of 2.5 µm as described in the online supplement. The axial spacing of the Tn3 reflection at 12.7 nm and the 6^{th} actin layer line at 5.9 nm was determined as described previously (45).

Molecular dynamics simulations

Human *TNNC2* with Ca^{2+} bound (holo) was modeled based on the Oryctolagus cuniculus holo (bound with four Ca^{2+} ions; two in each domain) troponin C (*Tnnc2*) X-ray crystal structure (PDB: 2TN4) (46). For modeling the human *TNNC2* Ca^{2+}-free state (apo), we again used an Oryctolagus cuniculus apo X-ray crystal structure (PDB: 1A2X) that was crystallized with a segment of C-terminal troponin I (TnI) (47). The CHARMM-GUI web server was used to build the solvated KCl-containing human *TNNC2* simulation systems (48). In total six systems were

built, three apo (Apo:WT, Apo:D34Y, and Apo:M79I) and three holo (Holo:WT, Holo:D34Y, Holo:M79I). Each system was simulated via all atom molecular dynamics (MD) using the Amber 18 MD simulation engine and the input files for conducting MD simulations were generated using CHARMM-GUI input generator (49, 50). The CHARMM36 all-atom additive force field parameters were used to parameterize all components of the system (51). We collected approximately 18μs of simulation data using a 2 fs time step. Additional details, including those for MD simulations with the intact troponin complex (PDB: 1J1E), are in the online supplement.

Myofiber contractility experiments

We adapted previously described methods to investigate the contractile properties of myofibers of patients (F1:P1, n = 19 fibers; F2:P1, n = 22 fibers) and healthy controls (N = 6, n = 78 fibers) (52–55). The protocol used in the current study is described in detail in the online supplement. After completion of the protocol the myofibers were stored for analysis of myosin heavy chain isoform composition.

Protein Expression and purification of fsTnC

An expression vector encoding human wild type and mutant (D34Y and M79I) troponin C were transformed into *E.coli* to express the proteins. A detailed description of the protein expression and purification protocol can be found in the online supplement.

Extraction and reconstitution of fsTnC in single permeabilized myofibers

Single myofibers were isolated and permeabilized as described above. We adapted previous methods (56) to reconstitute fsTnC in patient and control myofibers. The protocol for the reconstitution and for the contractile measurements during the reconstitution experiments are described in detail in the online supplement. After completion of the protocol the myofibers were stored for analysis of for myosin heavy chain isoform composition.

Effect of *tirasemtiv* on myofiber contractility

We tested the ability of *tirasemtiv*, a fast skeletal muscle troponin activator, to augment the contractile force of fast twitch patients' myofibers. Single myofibers were isolated and permeabilized as described above. The protocol was adapted from previous work (12). Details are in the online supplement.

Myosin heavy chain isoform composition of permeabilized myofibers

Determination of the myosin heavy chain isoform composition of the single myofibers used in the contractility assays was performed as described previously (53, 57). Details are in the online supplement.

Statistical analyses

The quantified histology and myofiber contractility data were tested for significance by performing a mixed model analysis with a random effect for biopsies and posthoc tests with a Bonferroni correction, after checking if the residues were normally distributed. The myofiber reconstitution and *tirasemtiv* data were tested for significance by a paired t test. Testing was performed using the software package SPSS Inc. (Armonk, NY, USA). A P-value less than 0.05 was considered significant.

Study approval

Patient Recruitment and Sample Collection

Written informed consents for study procedures and photographs were obtained by a qualified investigator (Protocol 12-N-0095 approved by the Institutional Review Board of the National Institute of Neurological Disorders and Stroke, National Institutes of Health). Clinical exome sequencing by the Radboudumc was approved by the Medical Review Ethics Committee, Region Arnhem–Nijmegen, Number 2011/188. All human subjects provided

595 informed consent for this study. The protocol for obtaining human biopsies from control
596 subjects was approved by the institutional review board at VU University Medical Center
597 (#2014/396) and written informed consent was obtained from the subjects.

AUTHOR CONTRIBUTIONS

ML: Conceived and designed the analysis, collected data, performed analyses, wrote the paper; SD: Collected data, performed analyses, wrote the paper; JW: wrote the paper; SC: collected data; LB: collected data; BK: collected data and performed analyses; PM: collected data and performed analyses; YH: Collected data and performed analyses; LM: Collected data and performed analyses; CQ: Collected data and performed analyses; SM: Collected data and performed analyses; RF: Collected data and performed analyses; GS: Collected data; DH: Provided compound, wrote the paper; FM: Provided compound, wrote the paper; TI: Collected data, performed analyses, wrote the paper; WM: Collected data and performed analyses; HG: wrote the paper; EJK: Collected data and performed analyses; KI: Collected data and performed analyses; PKH: Collected data and performed analyses; JP: Collected data and performed analyses; NV: Conceived and designed the analyses, collected data and performed analyses, wrote the paper; CB: Conceived and designed the analysis, collected data and performed analyses, wrote the paper; CO: Conceived and designed the analysis, collected data and performed analyses, wrote the paper.

ACKNOWLEDGEMENTS

We thank the families for participating in this study, and Christopher Mendoza and Gilberto ('Mike') Averion for their help in the clinic. We also thank the NIH Intramural Sequencing Center for performing the exome sequencing.

FUNDING

The Ottenheijm laboratory is supported by a ZonMW-VICI grant (91819613), H2020-MSCA-RISE-2014 (64568 'Muscle Stress Relief'), and a Muscle Dystrophy UK grant (16NEM-PG36-0111). JRP is supported by the NHLBI/NIH award HL128683. HLG is supported by NIAMS/NIH R01AR053897. Work in CG. Bönnemann's laboratory is supported by intramural funds by the NINDS/NIH. Exome sequencing was funded through the Clinical Center Genomics Opportunity

(CCGO), which is sponsored by the National Human Genome Research Institute (NHGRI), the NIH Deputy Director for Intramural Research, and the NIH Clinical Center. PKH was supported by the Maximizing Investigators' Research Award (MIRA) (R35) from NIGMS/NIH (R35GM124977) as well as supercomputer time from The Extreme Science and Engineering Discovery Environment (60).

REFERENCES

1. Gordon AM, Homsher E, Regnier M. Regulation of contraction in striated muscle. *Physiol Rev*. 2000;80(2):853-924. http://www.ncbi.nlm.nih.gov/pubmed/10747208

2. Li A, Nelson SR, Rahmanseresht S, et al. Skeletal MyBP-C isoforms tune the molecular contractility of divergent skeletal muscle systems. *Proc Natl Acad Sci U S A*. 2019;116(43):21882-21892. doi:10.1073/pnas.1910549116

3. Jungbluth H, Treves S, Zorzato F, et al. Congenital myopathies: Disorders of excitation-contraction coupling and muscle contraction. *Nat Rev Neurol*. 2018;14(3):151-167. doi:10.1038/nrneurol.2017.191

4. De Winter JM, Molenaar JP, Yuen M, et al. KBTBD13 is an actin-binding protein that modulates muscle kinetics. *J Clin Invest*. 2020;130(2):754-767. doi:10.1172/JCI124000

5. Solaro RJ, Lab M, Landesberg A, Burkhoff D, Ter Keurs H. Troponin C - Troponin I interactions and molecular signalling in cardiac myofilaments. In: *Advances in Experimental Medicine and Biology*. Vol 382. Springer New York LLC; 1995:109-115. doi:10.1007/978-1-4615-1893-8_12

6. Rarick HM, Tu X-H, Solaro RJ, Martin AF. *The C Terminus of Cardiac Troponin I Is Essential for Full Inhibitory Activity and Ca 2 Sensitivity of Rat Myofibrils**.; 1997. Accessed July 8, 2020. http://www.jbc.org/

7. Chandra M, Montgomery DE, Kim JJ, Solaro RJ. The N-terminal region of troponin T is essential for the maximal activation of rat cardiac myofilaments. *J Mol Cell Cardiol*. 1999;31(4):867-880. doi:10.1006/jmcc.1999.0928

8. Grabarek Z. Structural Basis for Diversity of the EF-hand Calcium-binding Proteins. *J Mol Biol*. 2006;359(3):509-525. doi:10.1016/j.jmb.2006.03.066

9. Gifford JL, Walsh MP, Vogel HJ. Structures and metal-ion-binding properties of the Ca2+-binding helix–loop–helix EF-hand motifs. *Biochem J*. 2007;405(2):199-221. doi:10.1042/BJ20070255

10. Oleszczuk M, Robertson IM, Li MX, Sykes BD. Solution structure of the regulatory domain of human cardiac troponin C in complex with the switch region of cardiac troponin I and W7: The basis of W7 as an inhibitor of cardiac muscle contraction. *J Mol Cell Cardiol*. 2010;48(5):925-933. doi:10.1016/j.yjmcc.2010.01.016

11. Takeda S, Yamashita A, Maeda K, Maeda Y. Structure of the core domain of human cardiac troponin in the Ca(2+)-saturated form. *Nature*. 2003;424(6944):35-41. doi:10.1038/nature01780

12. de Winter JM, Buck D, Hidalgo C, et al. Troponin activator augments muscle force in nemaline myopathy patients with nebulin mutations. *J Med Genet*. 2013;50(6):383-392. doi:10.1136/jmedgenet-2012-101470

13. Richards S, Aziz N, Bale S, et al. Standards and guidelines for the interpretation of sequence variants: A joint consensus recommendation of the American College of Medical Genetics and Genomics and the Association for Molecular Pathology. *Genet Med*. 2015;17(5):405-424. doi:10.1038/gim.2015.30

14. Johnston JJ, Kelley RI, Crawford TO, et al. A novel nemaline myopathy in the Amish caused by a mutation in troponin T1. *Am J Hum Genet*. 2000;67(4):814-821. doi:10.1086/303089

15. Sandaradura SA, Bournazos A, Mallawaarachchi A, et al. Nemaline myopathy and distal arthrogryposis associated with an autosomal recessive TNNT3 splice variant. *Hum Mutat*. 2018;39(3):383-388. doi:10.1002/humu.23385

16. Ilkovski B, Cooper ST, Nowak K, et al. Nemaline myopathy caused by mutations in the

797 muscle alpha-skeletal-actin gene. *Am J Hum Genet*. 2001;68(6):1333-1343.
798 doi:10.1086/320605

799 17. Laing NG, Wilton SD, Akkari PA, et al. A mutation in the alpha tropomyosin gene TPM3
800 associated with autosomal dominant nemaline myopathy. *Nat Genet*. 1995;9(1):75-79.
801 doi:10.1038/ng0195-75

802 18. Donner K, Ollikainen M, Ridanpää M, et al. Mutations in the β-tropomyosin (TPM2) gene
803 – a rare cause of nemaline myopathy. *Neuromuscul Disord*. 2002;12(2):151-158.
804 doi:10.1016/S0960-8966(01)00252-8

805 19. Pelin K, Hilpelä P, Donner K, et al. Mutations in the nebulin gene associated with
806 autosomal recessive nemaline myopathy. *Proc Natl Acad Sci U S A*. 1999;96(5):2305-
807 2310. doi:10.1073/pnas.96.5.2305

808 20. Yuen M, Sandaradura SA, Dowling JJ, et al. Leiomodin-3 dysfunction results in thin
809 filament disorganization and nemaline myopathy. *J Clin Invest*. 2015;125(1):456-457.
810 doi:10.1172/JCI80057

811 21. Agrawal PB, Greenleaf RS, Tomczak KK, et al. Nemaline myopathy with minicores
812 caused by mutation of the CFL2 gene encoding the skeletal muscle actin-binding
813 protein, cofilin-2. *Am J Hum Genet*. 2007;80(1):162-167. doi:10.1086/510402

814 22. Malfatti E, Böhm J, Lacène E, et al. A Premature Stop Codon in MYO18B is Associated
815 with Severe Nemaline Myopathy with Cardiomyopathy. *J Neuromuscul Dis*.
816 2015;2(3):219-227. doi:10.3233/jnd-150085

817 23. Miyatake S, Mitsuhashi S, Hayashi YK, et al. Biallelic Mutations in MYPN, Encoding
818 Myopalladin, Are Associated with Childhood-Onset, Slowly Progressive Nemaline
819 Myopathy. *Am J Hum Genet*. 2017;100(1):169-178. doi:10.1016/j.ajhg.2016.11.017

820 24. Ravenscroft G, Miyatake S, Lehtokari VL, et al. Mutations in KLHL40 Are a Frequent

Cause of Severe Autosomal-Recessive Nemaline Myopathy. *Am J Hum Genet*. 2013;93(1):6-18. doi:10.1016/j.ajhg.2013.05.004

25. Gupta VA, Ravenscroft G, Shaheen R, et al. Identification of KLHL41 mutations implicates BTB-Kelch-mediated ubiquitination as an alternate pathway to myofibrillar disruption in nemaline myopathy. *Am J Hum Genet*. 2013;93(6):1108-1117. doi:10.1016/j.ajhg.2013.10.020

26. Sambuughin N, Yau KS, Olivé M, et al. Dominant mutations in KBTBD13, a member of the BTB/Kelch family, cause nemaline myopathy with cores. *Am J Hum Genet*. 2010;87(6):842-847. doi:10.1016/j.ajhg.2010.10.020

27. Schiaffino S, Reggiani C. Fiber types in mammalian skeletal muscles. *Physiol Rev*. 2011;91(4):1447-1531. doi:10.1152/physrev.00031.2010

28. Hoh JFY. Laryngeal muscle fibre types. *Acta Physiol Scand*. 2005;183(2):133-149. doi:10.1111/j.1365-201X.2004.01402.x

29. Sandaradura SA, Bournazos A, Mallawaarachchi A, et al. Nemaline myopathy and distal arthrogryposis associated with an autosomal recessive *TNNT3* splice variant. *Hum Mutat*. 2018;39(3):383-388. doi:10.1002/humu.23385

30. Sung SS, Brassington AME, Grannatt K, et al. Mutations in genes encoding fast-twitch contractile proteins cause distal arthrogryposis syndromes. *Am J Hum Genet*. 2003;72(3):681-690. doi:10.1086/368294

31. Li C, Samulski RJ. Engineering adeno-associated virus vectors for gene therapy. *Nat Rev Genet*. 2020;21(4):255-272. doi:10.1038/s41576-019-0205-4

32. Salabarria SM, Nair J, Clement N, et al. Advancements in AAV-mediated Gene Therapy for Pompe Disease. *J Neuromuscul Dis*. Published online November 25, 2019:1-17. doi:10.3233/JND-190426

845 33. Kimura T, Ferran B, Tsukahara Y, et al. Production of adeno-associated virus vectors
846 for in vitro and in vivo applications. *Sci Rep*. 2019;9(1). doi:10.1038/s41598-019-49624-
847 w

848 34. Russell AJ, Hartman JJ, Hinken AC, et al. Activation of fast skeletal muscle troponin as
849 a potential therapeutic approach for treating neuromuscular diseases. *Nat Med*.
850 2012;18(3):452-455. doi:10.1038/nm.2618

851 35. Haus JM, Carrithers JA, Carroll CC, Tesch PA, Trappe TA. Contractile and connective
852 tissue protein content of human skeletal muscle: effects of 35 and 90 days of simulated
853 microgravity and exercise countermeasures. *Am J Physiol Integr Comp Physiol*.
854 2007;293(4):R1722-R1727. doi:10.1152/ajpregu.00292.2007

855 36. Hwee DT, Kennedy A, Ryans J, et al. Fast Skeletal Muscle Troponin Activator tirasemtiv
856 Increases Muscle Function and Performance in the B6SJL-SOD1G93A ALS Mouse
857 Model. Gillingwater TH, ed. *PLoS One*. 2014;9(5):e96921.
858 doi:10.1371/journal.pone.0096921

859 37. Lee EJ, Kolb J, Hwee DT, Malik FI, Granzier HL. Functional characterization of the intact
860 diaphragm in a Nebulin-based nemaline myopathy (NM) model-effects of the fast
861 skeletal muscle troponin activator tirasemtiv. *Int J Mol Sci*. 2019;20(20):5008.
862 doi:10.3390/ijms20205008

863 38. Shefner JM, Cudkowicz ME, Hardiman O, et al. A phase III trial of *tirasemtiv* as a
864 potential treatment for amyotrophic lateral sclerosis. *Amyotroph Lateral Scler Front*
865 *Degener*. 2019;20(7-8):584-594. doi:10.1080/21678421.2019.1612922

866 39. Andrews JA, Miller TM, Vijayakumar V, et al. CK-2127107 amplifies skeletal muscle
867 response to nerve activation in humans. *Muscle and Nerve*. 2018;57(5):729-734.
868 doi:10.1002/mus.26017

869 40. Shefner JM, Andrews JA, Genge A, et al. A Phase 2, Double-Blind, Randomized, Dose-
870 Ranging Trial Of Reldesemtiv In Patients With ALS. *Amyotroph Lateral Scler Front*
871 *Degener*. Published online 2020. doi:10.1080/21678421.2020.1822410

872 41. Teer JK, Green ED, Mullikin JC, Biesecker LG. VarSifter: Visualizing and analyzing
873 exome-scale sequence variation data on a desktop computer. *Bioinformatics*.
874 2012;28(4):599-600. doi:10.1093/bioinformatics/btr711

875 42. Karczewski KJ, Francioli LC, Tiao G, et al. The mutational constraint spectrum
876 quantified from variation in 141,456 humans. *Nature*. 2020;581(7809):434-443.
877 doi:10.1038/s41586-020-2308-7

878 43. Schindelin J, Arganda-Carreras I, Frise E, et al. Fiji: An open-source platform for
879 biological-image analysis. *Nat Methods*. 2012;9(7):676-682. doi:10.1038/nmeth.2019

880 44. Fischetti R, Stepanov S, Rosenbaum G, et al. The BioCAT undulator beamline 18ID: a
881 facility for biological non-crystalline diffraction and X-ray absorption spectroscopy at the
882 Advanced Photon Source. *J Synchrotron Radiat*. 2004;11(Pt 5):399-405.
883 doi:10.1107/S0909049504016760

884 45. Wakabayashi K, Sugimoto Y, Tanaka H, Ueno Y, Takezawa Y, Amemiya Y. X-ray
885 diffraction evidence for the extensibility of actin and myosin filaments during muscle
886 contraction. *Biophys J*. 1994;67(6):2422-2435. doi:10.1016/S0006-3495(94)80729-5

887 46. Houdusse A, Love ML, Dominguez R, Grabarek Z, Cohen C. Structures of four Ca2+-
888 bound troponin C at 2.0 Å resolution: Further insights into the Ca2+-switch int he
889 calmodulin superfamily. *Structure*. 1997;5(12):1695-1711. doi:10.1016/S0969-
890 2126(97)00315-8

891 47. Vassylyev DG, Takeda S, Wakatsuki S, Maeda K, Maéda Y. Crystal structure of troponin
892 C in complex with troponin I fragment at 2.3-Å resolution. *Proc Natl Acad Sci U S A*.

1998;95(9):4847-4852. doi:10.1073/pnas.95.9.4847

48. Jo S, Kim T, Iyer VG, Im W. CHARMM-GUI: A web-based graphical user interface for CHARMM. *J Comput Chem*. 2008;29(11):1859-1865. doi:10.1002/jcc.20945

49. Darden TA, Duke RE, Ghoreishi D, et al. AMBER 2018. Published online 2018.

50. Lee J, Cheng X, Swails JM, et al. CHARMM-GUI Input Generator for NAMD, GROMACS, AMBER, OpenMM, and CHARMM/OpenMM Simulations Using the CHARMM36 Additive Force Field. *J Chem Theory Comput*. 2016;12(1):405-413. doi:10.1021/acs.jctc.5b00935

51. Huang J, Rauscher S, Nawrocki G, et al. CHARMM36m: An improved force field for folded and intrinsically disordered proteins. *Nat Methods*. 2016;14(1):71-73. doi:10.1038/nmeth.4067

52. van de Locht M, Beecroft SJ, de Winter JM, et al. Recessive MYH7-related myopathy in two families. *Neuromuscul Disord*. 2019;29(6):456-467. doi:10.1016/j.nmd.2019.04.002

53. Joureau B, de Winter JM, Conijn S, et al. Dysfunctional sarcomere contractility contributes to muscle weakness in ACTA1-related nemaline myopathy (NEM3). *Ann Neurol*. 2018;83(2):269-282. doi:10.1002/ana.25144

54. Winter JM de, Joureau B, Lee E-JJ, et al. Mutation-specific effects on thin filament length in thin filament myopathy. *Ann Neurol*. 2016;79(6):959-969. doi:10.1002/ana.24654

55. Ottenheijm CAC, Buck D, de Winter JM, et al. Deleting exon 55 from the nebulin gene induces severe muscle weakness in a mouse model for nemaline myopathy. *Brain*. 2013;136(Pt 6):1718-1731. doi:10.1093/brain/awt113

916 56. Veltri T, De Oliveira GAP, Bienkiewicz EA, et al. Amide hydrogens reveal a temperature-
917 dependent structural transition that enhances site-II Ca 2+ -binding affinity in a C-
918 domain mutant of cardiac troponin C. *Sci Rep*. 2017;7(1). doi:10.1038/s41598-017-
919 00777-6

920 57. Ottenheijm CA, Witt CC, Stienen GJ, Labeit S, Beggs AH, Granzier H. Thin filament
921 length dysregulation contributes to muscle weakness in nemaline myopathy patients
922 with nebulin deficiency. *Hum Mol Genet*. 2009;18(13):2359-2369.
923 doi:10.1093/hmg/ddp168

924 58. SMART - Servier Medical ART. Accessed January 30, 2020. https://smart.servier.com/

925 59. Wittenbach JD, Cocanougher BT, Yun P, Foley AR, Bönnemann CG. MuscleViz: Free
926 open-source software for muscle weakness visualization. *J Neuromuscul Dis*.
927 2019;6(2):263-266. doi:10.3233/JND-190385

928 60. Towns J, Cockerill T, Dahan M, et al. XSEDE: Accelerating scientific discovery. *Comput*
929 *Sci Eng*. 2014;16(5):62-74. doi:10.1109/MCSE.2014.80

930

FIGURES

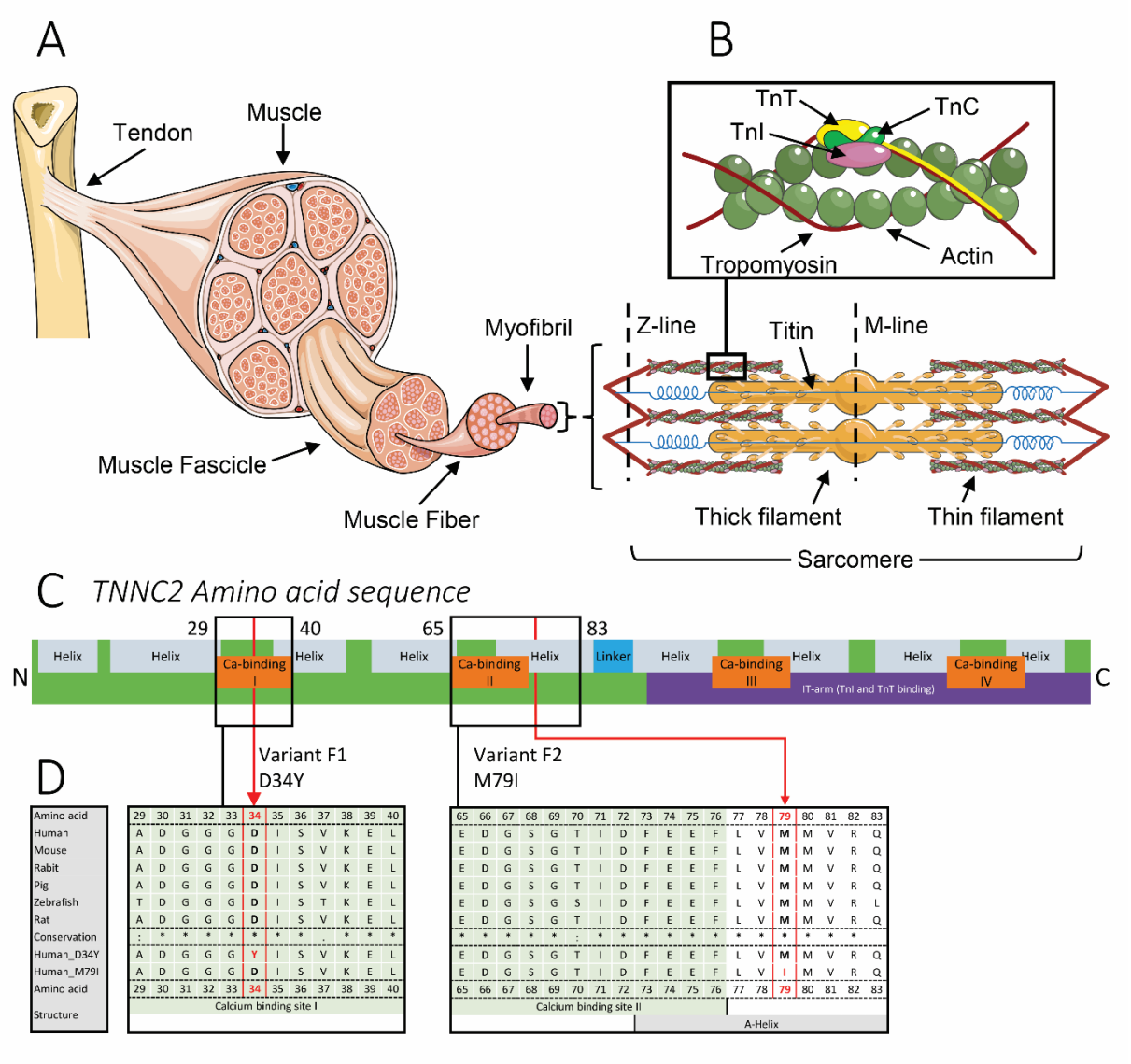

Figure 1. Muscle structure. **(A)** Sarcomeres are the smallest contractile units in muscle, consisting of myosin-based thick filaments and actin-based thin filaments decorated with the regulatory proteins troponin (Tn) and tropomyosin. **(B)** Magnification of the troponin complex, consisting of TnC, TnT and TnI, and tropomyosin on the actin-based thin filament. The images are modified from Servier Medical ART, licensed under a Creative Common Attribution 3.0 Generic License (58). **(C)** Schematic representation of the amino acid sequence of fsTnC; N = N-terminus; C = C-terminus. Both patient variants are indicated (F1:P1: c.100G>T; p.(Asp34Tyr), D34Y; F2:P1: c.237G>C; p.(Met79Ile); M79I) **(D)** Alignment of the fsTnC amino acid sequence in various species. The mutated residues are highlighted in red.

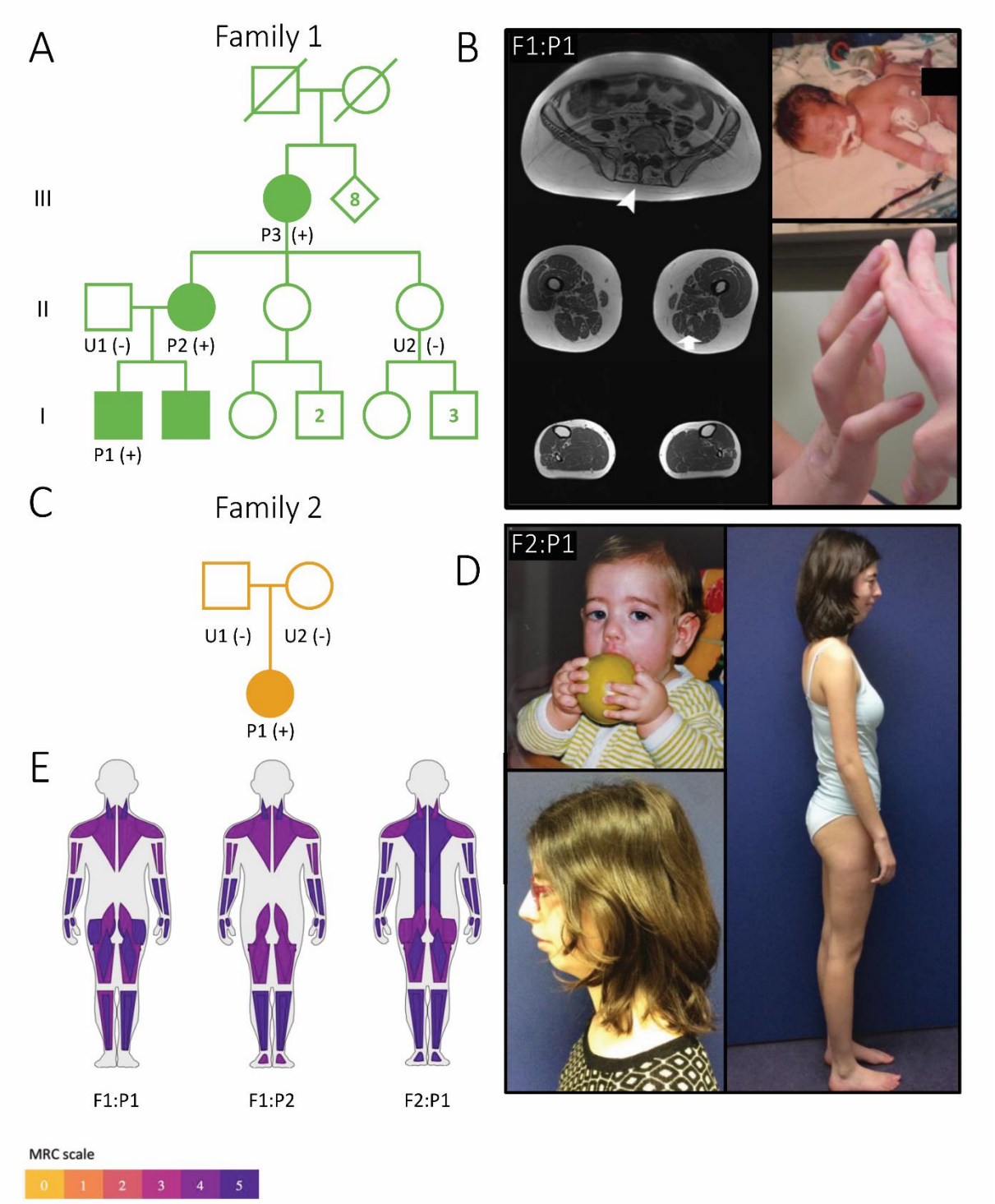

Figure 2. Pedigrees and clinical description of F1:P1 and F2:P1. **(A)** Pedigree of family 1 showing multiple affected relatives in different generations, consistent with autosomal dominant inheritance. (+) positive for the TNNC2 c.100G>T; p.D34Y missense variant by Sanger sequencing; (-) negative for TNNC2 c.100G>T; p.D34Y missense variant by Sanger

sequencing. Circles indicate female; squares indicate males; clinically affected relatives are shaded blue, unaffected relatives are shaded white **(B)** Muscle MRI imaging of F1:P1 (left). T1-axial images of the lower extremities show mild, focal fatty infiltration of different muscles in a patchy and heterogenous pattern (arrows). Paraspinal muscles are significantly affected in F1:P1 (top, arrowheads). Proximal thigh muscles (middle) are more affected than lower leg muscles (bottom). Photograph of F1:P1 at age 6 weeks with hypotonia and lower extremity weakness (top right). F1:P1 at age 26 years with contractures of the long finger flexors (bottom right). **(C)** Pedigree of family 2. **(D)** Photograph of F2:P1 as an infant indicating weakness in the facial muscles (top left). Photograph of F2:P1 at age 19 years with normal muscle mass and retrognathia. **(E)** Visualization of muscle weakness using MuscleViz (https://muscleviz.github.io), based on the MRC scores (59).

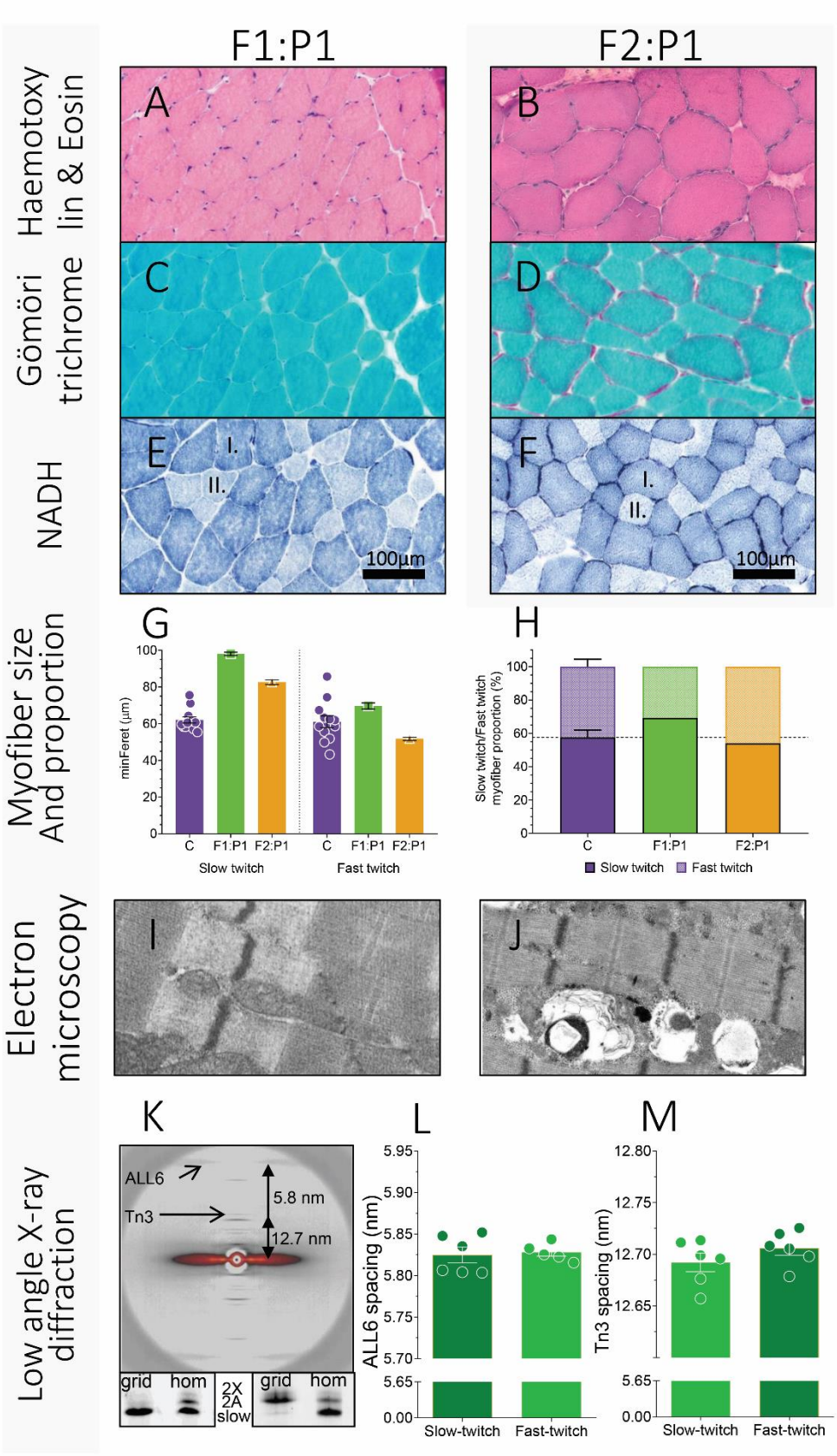
F1:P1
F2:P1
Haemotoxylin & Eosin
Gömöri trichrome
NADH
A
B
C
D
E
F
I.
II.
100µm
Myofiber size And proportion
G
H
minFeret (µm)
C
F1:P1
F2:P1
Slow twitch
Fast twitch
Slow twitch/Fast twitch myofiber proportion (%)
Electron microscopy
I
J
Low angle X-ray diffraction
K
L
M
ALL6
Tn3
5.8 nm
12.7 nm
grid
hom
2X 2A slow
ALL6 spacing (nm)
Tn3 spacing (nm)
Slow-twitch
Fast-twitch

625

Figure 3. Histology of F1:P1 spinal accessory muscle biopsy at age 16 years (left) and F2:P1 vastus lateralis muscle biopsy at age 9 years (right). **(A-B)** Hemotoxylin and eosin (H&E) staining shows mild myofiber size variability in both patients. **(C-D)** Gömöri trichrome stainings show no signs of nemaline rods in myofibers of both patients. **(E-F)** NADH stainings of muscle cross sections show larger slow twitch fibers (dark blue, indicated with **I.**) than fast twitch fibers (light blue, indicated with **II.**) in both patients. **(G)** Graph showing the myofiber minFeret of slow twitch versus fast twitch myofibers in control subjects (C), F1:P1 and F2:P1. **(H)** Graph showing the proportion of slow twitch versus fast twitch myofibers in control subjects (C), F1:P1 and F2:P1. The dark shading indicates the proportion of slow twitch fibers and the light shading indicates the proportion of fast twitch fibers. **(I-J)** Electron microscopy images show no abnormalities, and an intact myofibrillar structure in both patients. **(K)** Typical example of a low angle X-ray diffraction pattern obtained from twenty-eight fast twitch myofibers of F1:P1 mounted and aligned in one plane between two-halves of an electron microscopy grid. Note the well resolved equatorial and meridional reflections. Arrows indicate the ALL6 and Tn3 reflections. Bottom: myosin heavy chain isoform composition of the myofibers in the grids, showing successful segregation of fast- and slow twitch fibers from F1:P1. Spacing of the actin layer line 6 reflection (ALL6; **(L)**) and the Tn3 reflection **(M)** are comparable between slow- and fast twitch myofibers. Each dot represents data from one set of grids containing 28 myofibers. Data is depicted as mean ± SEM.

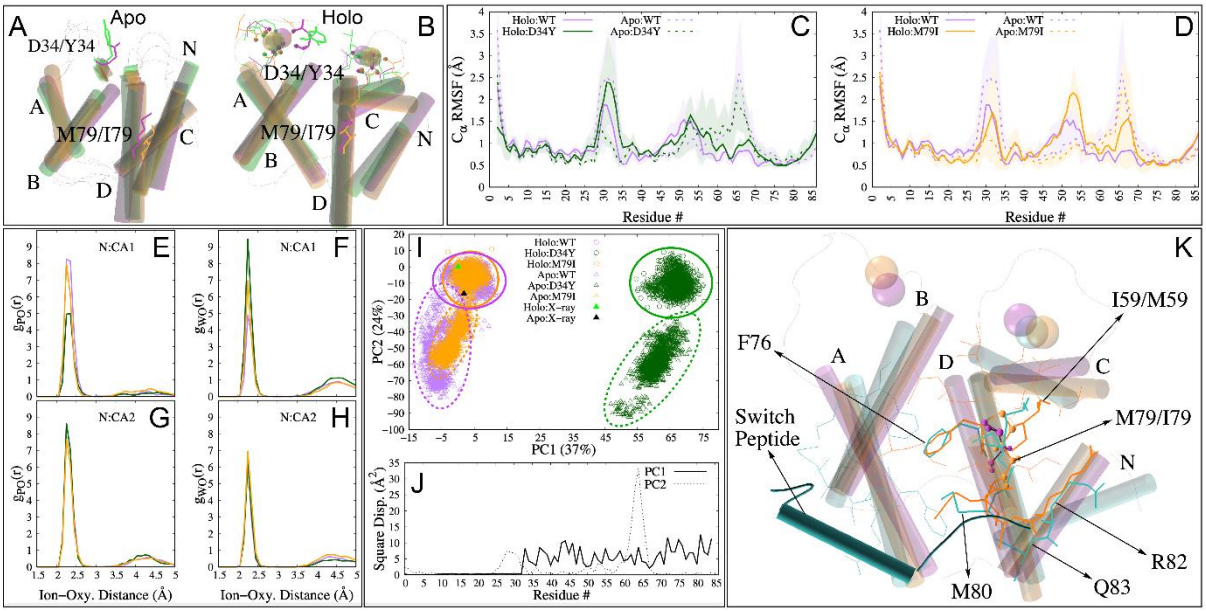

Figure 4. Results of the molecular dynamics simulations. (**A-B)** Superposition of N-domains of MD predicted apo (A) and holo (B) variants. WT, D34Y and M79I variants are colored purple, green and orange respectively. Helices N (residues 2-11), A (residues 14-27), B (residues 40-48), C (residues 54-63), and D (residues 74-85) of the N-domain are labeled. Protein oxygens within 2.5Å of Ca^{2+} are shown as spheres and their respective residues in sticks. (**C-D)** Root mean squared fluctuations (RMSF) of N-terminal domain residues. Holo and apo systems are represented as lines and broken lines respectively. WT is compared against D34Y and M79I in panels C and D respectively. Shaded regions reflect standard deviations. (**E-H)** Radial distribution of protein (E,G) and solvent (F,H) oxygens about bound Ca^{2+} ions in the fsTnC N-terminal domains from the final 50 ns of each trajectory. **(I-J)** Principal component (PC) analysis of the fsTnC2 N-domain MD trajectory data (J). Square displacements signify the relative contribution of each amino acid to PC1 (solid) or PC2 (dashed) (K). PC1 reflects the displacement of helices B-D, while PC2 corresponds to the loop connecting the C and D helices. These PCs demonstrate that the apo structures exhibit different displacements, or conformations, than the holo structures, and the D34Y variant samples a very different conformation than the WT and the M79I variants. **(K)** Cartoon diagram of the MD-predicted structures for holo WT fsTnC (purple); holo M79I fsTnC (orange); holo cTnC with switch

peptide (cyan). The structures of WT and M79I fsTnC are from the MD simulations; for cTnC the PDB 1MXL structure was used. Residues that are within 4Å of the TnI switch peptide in cTnC are shown as cyan sticks, and residues within 4Å of M79/I79 in holo M79I fsTnC are shown as orange sticks. Residues that overlap between the two are shown as thick sticks. M79/I79 is shown in ball and stick representation.

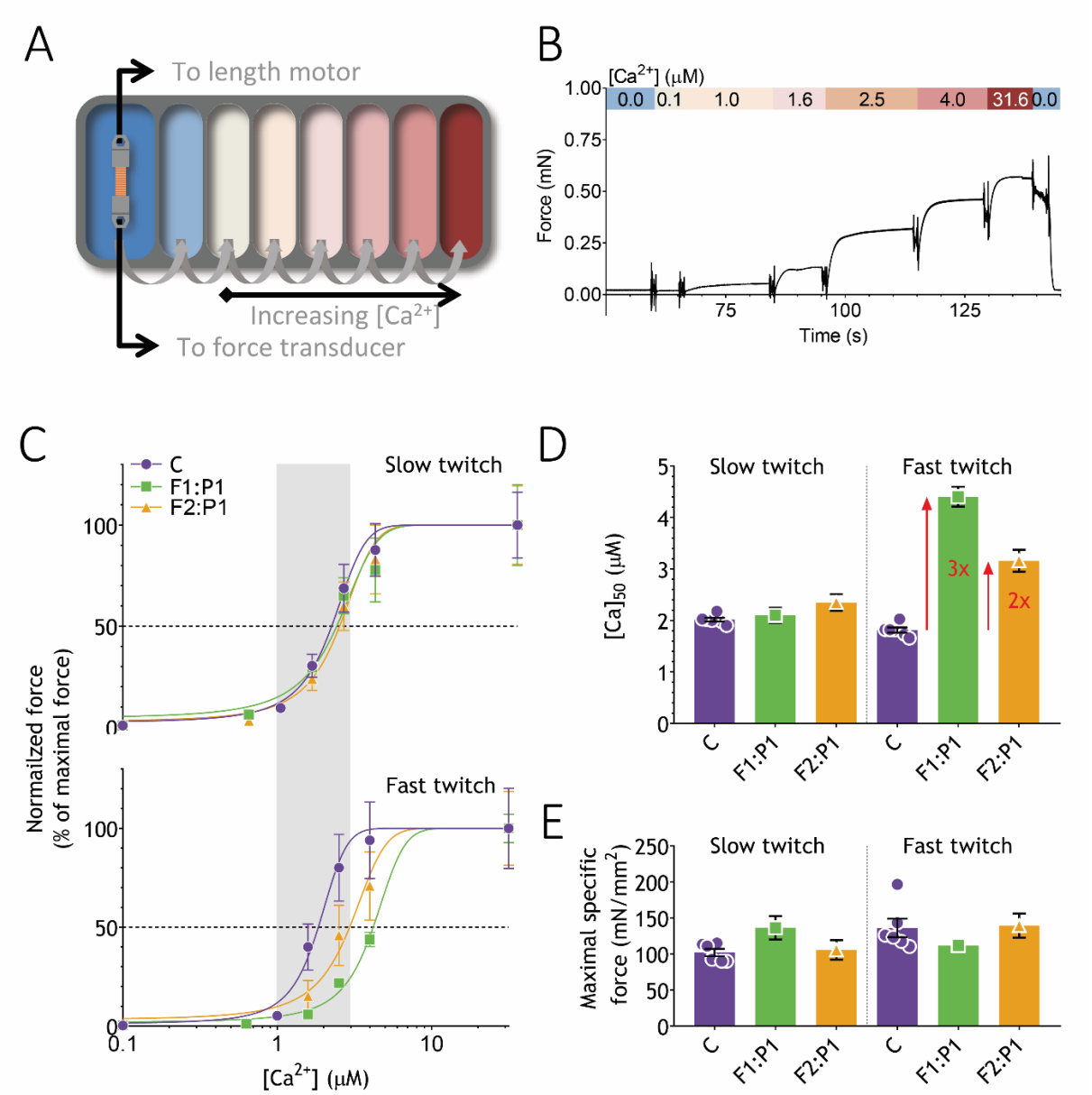

Figure 5. The experimental design and results of the myofiber contractility experiments. **(A)** Schematic representation of the contractility setup. An isolated single myofiber between aluminum T-clips is mounted between a force transducer and length motor. The fiber is subsequently passed through the baths filled with solutions with incremental [Ca^{2+}]. **(B)** Typical tracing showing the force response to the incremental Ca^{2+}-concentrations, followed by the protocol in which a rapid release and restretch (k_{TR}) and short-length perturbations (active stiffness) were imposed on the myofibers (Ca^{2+}-concentrations, k_{TR} and active stiffness are indicated in the colored bar). Data shown is from a control myofiber (fast twitch,

CSA=0.0054mm^2). **(C)** The force-[Ca^{2+}] relation, showing the average of all slow twitch (top) and fast twitch (bottom) control myofibers versus the slow twitch and fast twitch myofibers from F1:P1 and F2:P1. The physiological [Ca^{2+}] range is indicated by the gray bar. **(D)** The [Ca^{2+}] at which 50% of maximum force is reached. **(E)** The maximum force normalized to myofiber cross-sectional area (i.e. specific force). Data is depicted as mean ± SEM.

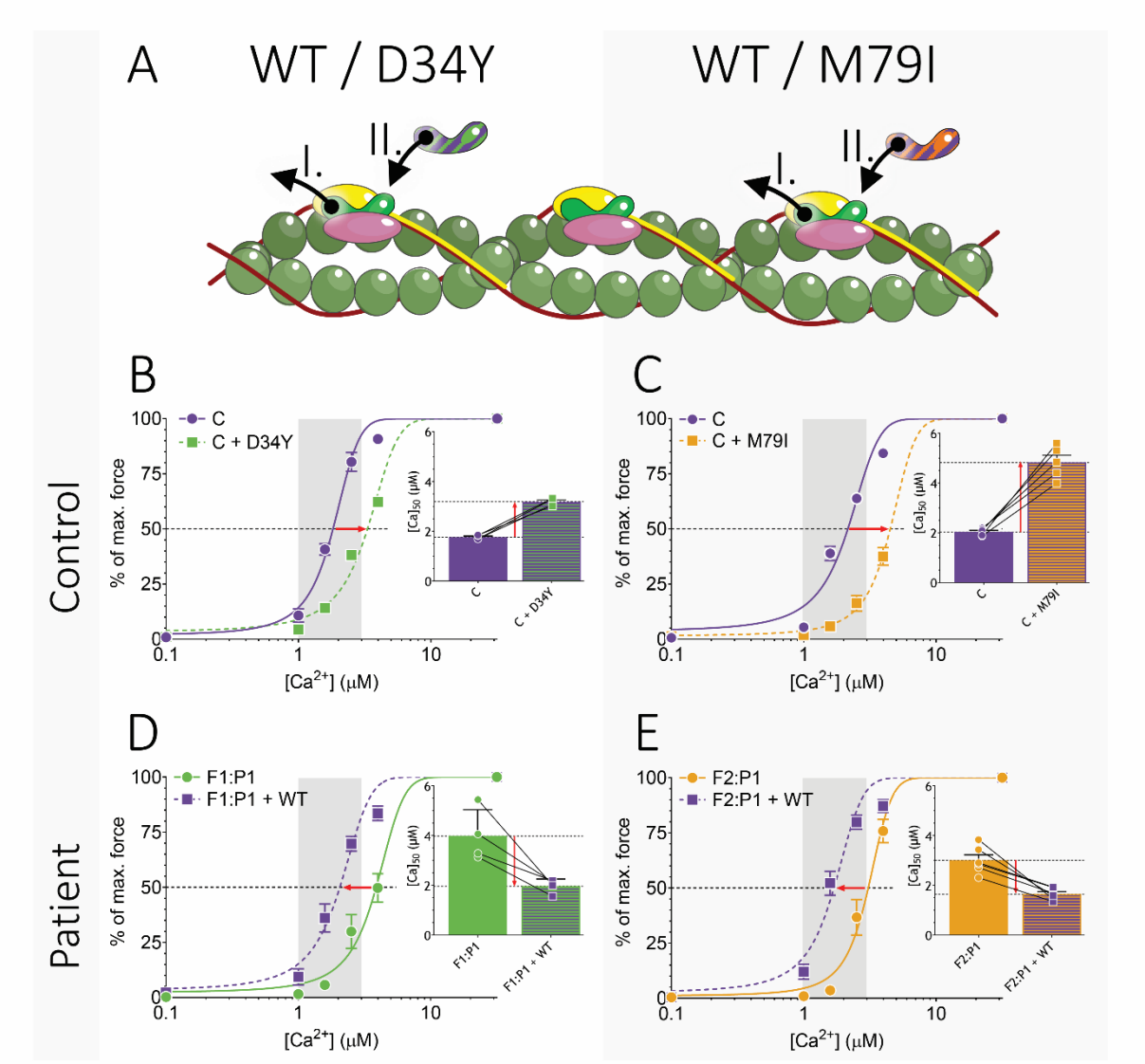

Figure 6. The experimental design and results of the reconstitution of myofibers with recombinant fsTnC. **(A)** The schematic depicts the thin filament with troponin complex in which (**I)** endogenous fsTnC is removed from fast twitch myofibers, followed by (**II)** reconstitution with exogenous fsTnC. **(B-C)** Normalized force-[Ca^{2+}] relation relations of myofibers from control subjects before and after reconstitution with recombinant D34Y-fsTnC (B) and M79I-fsTnC (C). Inset shows the [Ca^{2+}] at which 50% of maximum force is reached **(D-E)** Normalized force-[Ca^{2+}] relation relations of myofibers from F1:P1 (D) and F2:P1 (E) before and after reconstitution with recombinant WT-fsTnC. Inset shows the [Ca^{2+}] at which 50% of maximum

691 force is reached. The physiological [Ca^{2+}] range is indicated by the gray bar. Data are depicted

692 as mean ± SEM.

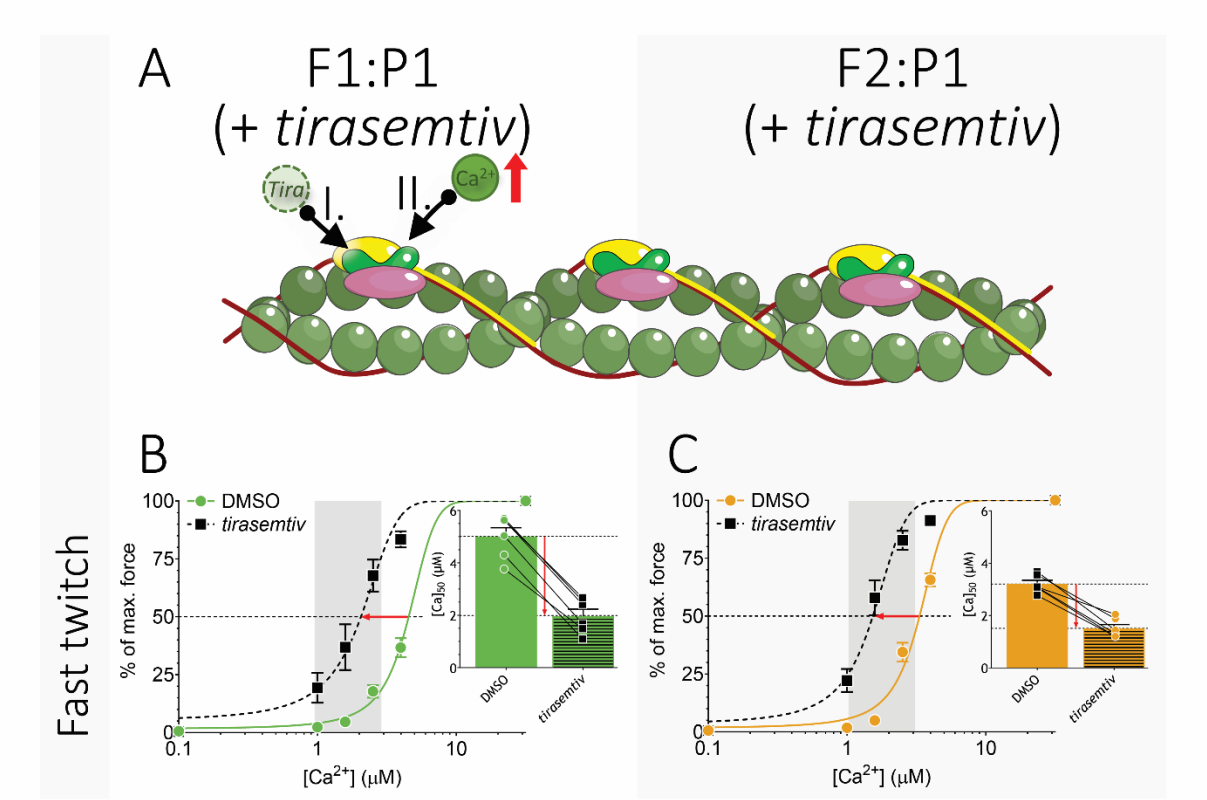

693

694 **Figure 7.** Experimental design and results for myofibers of controls (C), F1:P1 and F2:P2
695 exposed to DMSO and *tirasemtiv*. **(A)** Schematic depiction of a thin filament section including
696 one troponin subunit illustrating the Ca^{2+} sensitizing effect of *tirasemtiv*: **I.** *Tirasemtiv* is added
697 to the pCa solution **II.** enhancing Ca^{2+} binding to troponin in fast twitch myofibers. **(B-C)**
698 Normalized force-[Ca^{2+}] relations of fast twitch myofibers of F1:P1 (D) and F2:P1 (E) before
699 and during exposure to 10 µM *tirasemtiv*. Inset shows the [Ca^{2+}] at which 50% of maximum
700 force is reached. The physiological [Ca^{2+}] range is indicated by the gray bar. Data are depicted
701 as mean ± SEM.

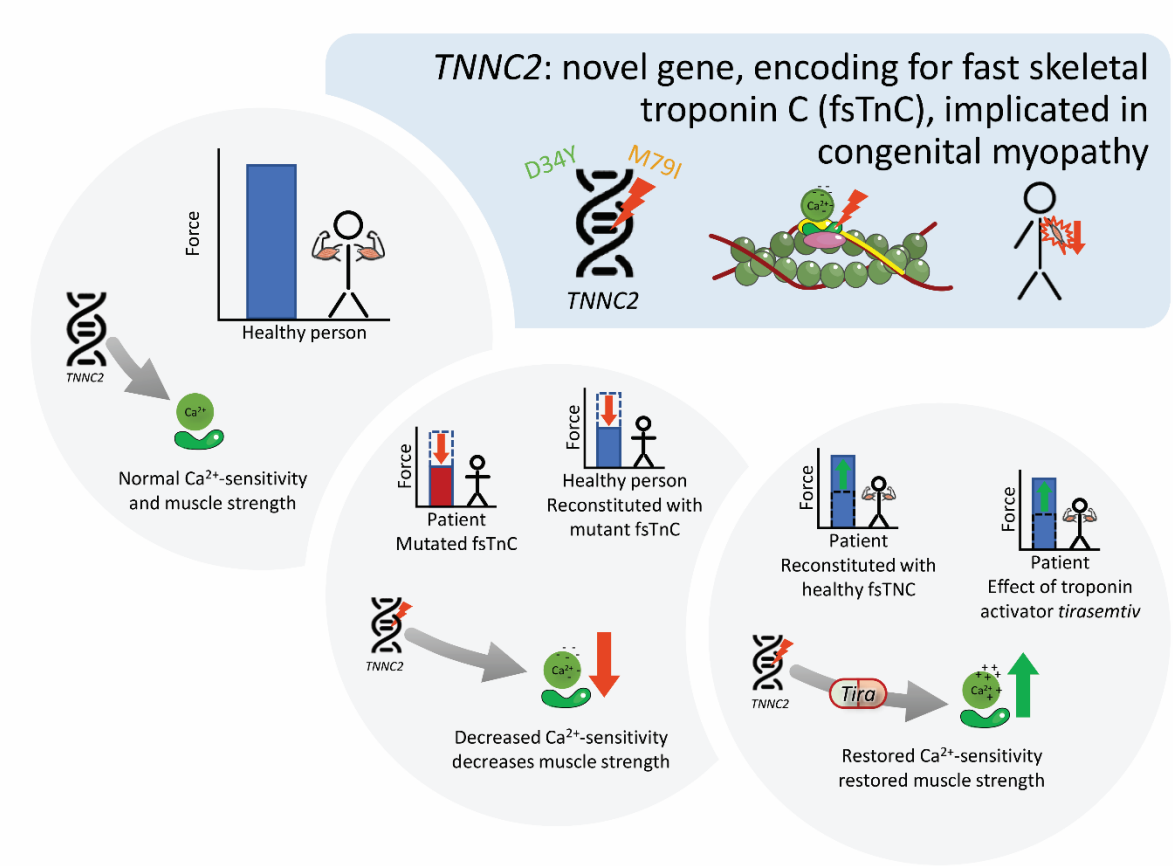

Figure 8. Graphic summary of the pathomechanism in *TNNC2*-related congenital myopathy.

TABLES

Table 1. Detailed clinical description of family 1 (F1) and family 2 (F2). F1:P1 indicates patient 1 from family 1, etc. M = male; F = female; yrs = years; mo = months; PEG = percutaneous endoscopic gastrostomy; CK = creatine kinase; EMG = electromyography; Rep Stim = Repetitive stimulation; FVC = forced vital capacity; NP = not performed; LE = lower extremity; MRI = Magnetic Resonance Imaging, EM = electron microscopy.

CLINICAL PHENOTYPE				
Family/Patient	**F1:P1**	**F1:P2**	**F1:P3**	**F2:P1**
Ethnicity	Caucasian	Caucasian	Caucasian	Caucasian
Sex/age at last examination (yrs.)	M/26	F/55	F/76	F/19
TNNC2 mutation	c.100G>T; p.Asp34Tyr	c.100G>T; p.Asp34Tyr	c.100G>T; p.Asp34Tyr	c.237G>C; p.Met79Ile
Inheritance	Dominant	Dominant	Presumed de novo	De novo

Onset	Maternal polyhydramnios treated with serial amniocenteses; hypotonia, vocal cord paralysis, respiratory insufficiency requiring intubation and tracheostomy at birth; PEG tube due to gastroesophageal reflux concerns; camptodactyly with contractures bilaterally and small right ear canal.	Respiratory failure due to stridor and vocal cord paralysis requiring intubation and tracheostomy at birth; scoliosis by 8 days.	Breech presentation; difficulties breathing at birth.	Maternal polyhydramnios treated with serial amniocenteses; reduced fetal movements; severe hypotonia; respiratory weakness; difficulties swallowing requring PEG tube at 4mo.
Motor development	Delayed; rolled 10 mo, walked independently 17 mo; difficulties keeping up with peers.	Delayed; sat unsupported 8 mo; rolled 1 yr, walk with support 15 mo; never able to run; difficulty keeping up with peers.	Delayed; walked independently 15 mo; climb stairs and jump 6 yrs; never able to run.	Standing age 1 yrs, walked independently age 1.5 yrs. Difficulty keeping up with peers; frequent falls. Unable to run.
Muscle weakness	Improved over time; axial, proximal and distal weakness 4-/5 – 5/5 range (MRC-grade) (26 yrs); progressive scoliosis requiring spinal fusion surgery with rod placement (16 yrs).	Stable with gradual decline recently; axial, proximal and distal weakness 4-/5 – 5/5 range (55 yrs) (MRC-grade); mild scoliosis.	Stable with gradual decline recently; mildly reduced 4/5 – 5/5 range (76yrs) (MRC-grade); scoliosis requiring surgery with bone fusions.	Mild proximal weakness 4/5 (MRC grade).
Gait	Waddling gait, unable to get up from a squatting position.	Waddling gait.	Kyphotic posture.	Normal gait, unable to walk on heels or toes. Difficulties with stairs.

Facial involvement	Mild upper and lower facial weakness; ptosis and ophthalmoplegia (childhood).	Mild upper and lower facial weakness; progressive ptosis and ophthalmoplegia (childhood).	Facial weakness, ophthalmoplegia, no ptosis.	Facial weakness; diplopia lateroflexion to the left, increases with fatigue.
Respiratory involvement (age)	FVC 45% predicted (26 yrs).	FVC 73% predicted; 11% decline from sitting to supine (55 yrs).	Tracheoesophageal fistula with pneumonias (74 yrs); FVC 47% predicted (76 yrs).	Recurrent pneumonias until age 3 yrs. FVC 76% predicted (19 yrs).
Cardiac involvement (age)	Echocardiogram normal (26 yrs).	Echocardiogram normal (55 yrs).	Moderate tricuspid regurgitation and trivial pericardial effusion (76 yrs).	Normal electrocardiogram (19 yrs).
Cognitive involvement	Learning disability, graduated high school.	Mild learning disability, graduated high school.		Normal.
EMG/Rep stim (age)	Chronic myopathic process/normal.	NP	NP	NP
Histology (age, muscle biopsied)	Mild variation in fiber size with mild fiber type 2 atrophy; No ultrastructural abnormalities on EM (16 yrs, spinal accessory muscle).	NP	NP	Increase of type 1 fibers, small type 2 fibets, No ultrastructural abnormalities on EM (8 yrs, quadriceps).

LE MRI imaging (age)	Mild, focal fatty infiltration of lower extremity muscles in a patchy and heterogenous pattern. Paraspinal muscles are significantly affected; proximal thigh muscles are less affected than lower leg muscles (26 yrs).	Mild, focal fatty infiltration of lower extremity muscles in a patchy and heterogenous pattern. Proximal thigh muscles are less affected than lower leg muscles (55 yrs).	Mild, focal fatty infiltration of lower extremity muscles in a patchy and heterogenous pattern. Paraspinal muscles are significantly affected; proximal thigh muscles are less affected than lower leg muscles (76 yrs).	Normal (19 yrs)
Other	Long-standing history of poor appetite and difficulty gaining weight; osteopenia (5 yrs).	generalized pain; Osteopenia (5 yrs).	Osteopenia with 6 bone fractures.	Generalized hypermobility (Beighton 6/9).

709

Table 2. Basic information of control subjects, F1:P1 and F2:P1.

BASIC CLINICAL INFORMATION								
Biopsy	**Patient ID**	**Mutation**	**Gender**	**Age at last investigation (yrs)**	**Age at biopsy (yrs)**	**Height (cm)**	**Weight (kg)**	**BMI**
Control	1	N/A	Male	N/A	44	177	83	26.64
Control	2	N/A	Male	N/A	50	192	117.7	32.1
Control	3	N/A	Male	N/A	50	180	83	25.76
Control	4	N/A	Female	N/A	65	166	66.5	24.13
Control	5	N/A	Female	N/A	53	174	64	21.14
Control	6	N/A	Female	N/A	51	171	68	23.26
Patient	F1:P1	D34Y	Male	26	16	N/A	N/A	N/A
Patient	F2:P1	M79I	Female	21	19	N/A	N/A	N/A

Table 3. Myofiber morphology, quantified from histology images. Data is depicted as mean ± SEM.

MYOFIBER MORPHOLOGY										
Subject		**C**	**(N/n)**	**F1:P1**	**(N/n)**	**%**	***p-value***	**F2:P1**	**(N/n)**	**%**	***p*-value**
minFeret diameter slow twitch fibers	µm	60.0 ± 0.6	(12/192)	97.5 ± 1.1	(1/282)	163%	**0.001**	81.9 ± 1.4	(1/125)	137%	**0.023**
minFeret diameter fast twitch fibers	µm	49.3 ± 0.9	(12/110)	66.6 ± 1.4	(1/125)	135%	0.193	51.7 ± 0.9	(1/108)	105%	0.348
Proportion slow twitch fibers	%	57.6 ± 4.4	(12/192)	69.3	(1/282)	12%	N/A	53.6	(1/125)	-4%	N/A
Proportion fast twitch fibers	%	42.4 ± 4.4	(12/110)	30.7	(1/125)	-12%	N/A	46.4	(1/108)	4%	N/A

Table 4. Contractility data of slow- and fast-twitch myofibers of control subjects (C) and F1:P1 and F2:P1. All data are depicted as mean ± SEM. The number of measured biopsies (N) and single myofibers (n) is shown, as well as the percentage change (%) of patient compared to control and the p-value. n_{Hill} = Hill coefficient.

SLOW TWITCH MYOFIBERS										
Subject		**C**	**(N/n)**	**F1:P1**	**(N/n)**	**%**	***p-value***	**F2:P1**	**(N/n)**	**%**	***p-value***
Max. force normalized to CSA	mN/mm^2	102.1 ± 5	(6/39)	136.4 ± 16.2	(1/2)	34%	0.131	105.9 ± 13.5	(1/7)	4%	0.845
$[Ca^{2+}]_{50}$	µM	0.00202 ± 0.00004	(6/37)	0.0021 ± 0.00015	(1/2)	4%	0.548	0.00235 ± 0.00016	(1/10)	16%	**0.029**
n_{Hill}	..	3.26 ± 0.1	(6/37)	2.39 ± 0.17	(1/2)	-27%	0.330	3.43 ± 0.27	(1/10)	5%	0.872
FAST TWITCH MYOFIBERS										
Subject		**C**	**(N/n)**	**F1:P1**	**(N/n)**	**%**	***p-value***	**F2:P1**	**(N/n)**	**%**	***p-value***
Max. force normalized to CSA	mN/mm^2	136.3 ± 12.9	(6/31)	111.9 ± 7.9	(1/16)	-18%	0.332	139.5 ± 16.7	(1/10)	2%	0.350
$[Ca^{2+}]_{50}$	µM	0.00181 ± 0.00005	(6/39)	0.0044 ± 0.00019	(1/16)	143%	**0.000**	0.00316 ± 0.00021	(1/12)	75%	**0.000**
n_{Hill}	..	4.43 ± 0.36	(6/39)	2.63 ± 0.07	(1/16)	-41%	**0.029**	3.23 ± 0.22	(1/12)	-27%	0.086